

Expressive riverine fluxes over Amazon floodplain units revealed by high resolution 2D modelling

Alice César Fassoni-Andrade¹, Rodrigo Cauduro Dias de Paiva², Sly Wongchuig³, Claudio Clemente Faria Barbosa⁴, and Fabien Durand⁵

¹Instituto de Pesquisas Hidráulicas IPH, Universidade Federal do Rio Grande do Sul UFRGS

²Instituto de Pesquisas Hidráulicas IPH, Universidade Federal do Rio Grande do Sul UFRGS, Porto Alegre, Brazil

³Univ. Grenoble Alpes, IRD, CNRS, Grenoble INP, Insitut des Géosciences de l'Environnement (IGE, UMR 5001)

⁴Brazilian Institute of Space Research

⁵IRD/LEGOS

November 24, 2022

Abstract

Water fluxes in the Amazon River floodplain affect hydrodynamic and ecological processes from local to global scales. Nevertheless, these fluxes remain poorly understood due to difficult access and limited data. In this study, we characterize the hydrodynamics of eight floodplain units of the central Amazon River (40'000 km²) using the 2D hydraulic model HEC-RAS. High resolution modeling improved the representation of river and floodplain discharge, water surface elevation (77 cm accuracy) and flood extent (~80% - high water period, ~52% -low water period). We have learned 13 lessons about river and floodplain hydrodynamics from the modeling. The most remarkable lessons are that the floodplain is organized in units of about 80 km with upstream inflow and downstream outflow. These gross flows are much larger than the net flows with values of up to 20% of the Amazon River discharge and a residence time around 6 days during floods (several months during low water period). Water extent does not have strong interannual variability during floods as the volume stored in the floodplain, possibly due to topographic constrains. Significant flood extent and volume hysteresis, as well as active flow and storage zones on the floodplain, highlight the complexity of floodplain hydrodynamics. Extreme floods strongly impact the onset and duration of the flood of up to 2 months and, consequently, on the period of high connectivity with the river. These findings are important for understanding carbon and sediment fluxes, and the effects of climate change on water fluxes and riparian communities.

Expressive riverine fluxes over Amazon floodplain units revealed by high resolution 2D modelling

Alice César Fassoni-Andrade^{1,2*}, Rodrigo Cauduro Dias de Paiva¹, Sly Wongchuig³, Claudio Barbosa⁴, Fabien Durand^{2,5}

¹ Institute of Hydraulic Research, Federal University of Rio Grande do Sul (UFRGS), Porto Alegre, Brazil.

² Institute of Geosciences, University of Brasília (UnB), Campus Universitário Darcy Ribeiro, Brasília, Brazil.

³ Univ. Grenoble Alpes, IRD, CNRS, Grenoble INP, Institut des Géosciences de l'Environnement (IGE, UMR 5001), 38000, Grenoble, France.

⁴ Instrumentation Lab for Aquatic Systems (LabISA), Earth Observation Coordination of National Institute for Space Research (INPE), São José dos Campos, SP, Brazil.

⁵ Laboratoire d'Etudes en Géophysique et Océanographie Spatiales (LEGOS), Université Toulouse, IRD, CNRS, CNES, UPS, Toulouse, France.

*Corresponding author: Alice Fassoni-Andrade (alice.fassoni@unb.br, alice.fassoni@gmail.com)

Key Points:

- Improved representation of Amazon River/floodplain hydrodynamics from 2D high resolution model
- Floodplain hydrodynamic complexity with flood extent reaching a plateau during floods and significant flood extent and volume hysteresis
- Expressive inflow/outflow over floodplain units of around 80 km, representing up to 20% of the Amazon River discharge

Abstract

Water fluxes in the Amazon River floodplain affect hydrodynamic and ecological processes from local to global scales. Nevertheless, these fluxes remain poorly understood due to difficult access and limited data. In this study, we characterize the hydrodynamics of eight floodplain units of the central Amazon River (40'000 km²) using the 2D hydraulic model HEC-RAS. High resolution modeling improved the representation of river and floodplain discharge, water surface elevation (77 cm accuracy) and flood extent (~80% - high water period, ~52% -low water period). We have learned 13 lessons about river and floodplain hydrodynamics from the modeling. The most remarkable lessons are that the floodplain is organized in units of about 80 km with upstream inflow and downstream outflow. These gross flows are much larger than the net flows with values of up to 20% of the Amazon River discharge and a residence time around 6 days during floods (several months during low water period). Water extent does not have strong interannual

38 variability during floods as the volume stored in the floodplain, possibly due to topographic
39 constrains. Significant flood extent and volume hysteresis, as well as active flow and storage
40 zones on the floodplain, highlight the complexity of floodplain hydrodynamics. Extreme floods
41 strongly impact the onset and duration of the flood of up to 2 months and, consequently, on the
42 period of high connectivity with the river. These findings are important for understanding carbon
43 and sediment fluxes, and the effects of climate change on water fluxes and riparian communities.

44
45

1. Introduction

46 The Amazon is the largest river system in the world, both in terms of the drainage area
47 and discharge. Their seasonal flood pulse induces a large annual variation in water surface
48 elevation in the floodplain and flooded area. The water level amplitude can reach up to 13 m
49 (Birkett et al., 2002) and the water surface extent of the basin varies between 284'200 km² and
50 633'500 km² during the high (April-May) and low water (October-November) periods,
51 respectively (Fleischmann et al., 2022; Hess et al., 2015). Moreover, the bidirectional flows and
52 water residence time in the floodplain are dynamic in space and time, and the patterns of water
53 surface elevation variation are complex (Alsdorf et al., 2007; Cao et al., 2018). The Amazon
54 River flood also has a great influence on regional and global processes, such as sediment
55 transport (Armijos et al., 2020; Dunne et al., 1998), local geomorphology (Fricke et al., 2019;
56 Latrubesse & Franzinelli, 2002), vegetation distribution (Ferreira-Ferreira et al., 2014), seed
57 dispersal (Melack et al., 2009), carbon dioxide (Abril et al., 2014) and methane emissions (Basso
58 et al., 2021), and commercial and subsistence fisheries (Duponchelle et al., 2021). Therefore,
59 understanding the water flow between the Amazon River and floodplain is of great importance to
60 better understand these processes.

61 Due to the extent of the Amazon River floodplain (about 20 to 50 km wide) and its
62 difficult access, in situ measurements of topography, water level, and water flow are limited. The
63 detailed hydrodynamics of the river-floodplain system and the ecological function of the
64 floodplain are therefore poorly known. Hydrologic and hydrodynamic models have been applied
65 to the Amazon basin to understand large-scale hydrodynamics processes and the role of
66 floodplains (Beighley et al., 2009; Coe et al., 2008; Correa et al., 2017; Getirana et al., 2012; Luo
67 et al., 2017; Paiva et al., 2013; Sorribas et al., 2020; Yamazaki et al., 2011). These studies
68 showed that the water flow exchanged between the river and the floodplain has the same order of
69 magnitude as the river discharge (about 10⁴ to 10⁵ m³s⁻¹; Sorribas et al., 2020) and can represent
70 between 3% and 40% of the river discharge depending on the period (Getirana et al., 2012;
71 Richey et al., 1989; Sorribas et al., 2020; Wilson et al., 2007). Water stored in floodplains, which
72 can have a residence time of more than 300 days (Sorribas et al., 2020), plays an important role
73 in delaying and attenuating the river's flood wave (Getirana et al., 2012; Paiva et al., 2013;
74 Yamazaki et al., 2011). Although these models adequately represent river hydraulics (e.g., full
75 Saint-Venant equation, particle-tracking model), they are simplified to represent floodplain
76 hydrodynamics, such as bidirectional flows, which can be better represented with two-
77 dimensional numerical models.

78 Regional applications of two-dimensional hydraulic models allowed better representation
79 of the floodplain hydrodynamics, such as the study by Wilson et al. (2007), where the water
80 exchange between the Amazon River and the adjacent floodplain over a 240 km-long reach was
81 evaluated. As the drainage process in the floodplain in this model was poorly represented due to

82 errors in the topographic data (Wilson et al., 2007), Yamazaki et al. (2012) and Baugh et al.
83 (2013) have improved the accuracy of this simulation with correction of topographic errors.
84 Despite the improvement, these studies considered the SRTM3 digital elevation model (DEM) in
85 open water areas, where the lakes are represented by a flat surface. The topography of the
86 extensive central Amazon floodplain is difficult to represent using global elevation models, since
87 it is complex and composed of many interconnected lakes and channels (Trigg et al., 2012) and
88 vegetation types (Hess et al., 2015). In addition, Baugh et al. (2013), Paiva et al. (2013),
89 Yamazaki et al. (2012) and Getirana et al. (2012) point out that topography is the main source of
90 uncertainty in modeling flows in the river-floodplain system, as well as being difficult to access.

91 The bathymetry of lakes Calado (73 km²; Lesack & Melack, 1995), Lago Grande de
92 Curuai (2440 km²; Barbosa et al., 2006) and Janauacá (786 km²; Pinel et al., 2015) were
93 estimated in situ, allowing the implementation of local two-dimensional models and expanding
94 the knowledge regarding the hydrology of river-floodplain systems (Bonnet et al., 2008, 2017; Ji
95 et al., 2019; Lesack & Melack, 1995; Pinel et al., 2019; Rudorff et al., 2014a, 2014b).
96 Floodplains' water residence times estimated by local models range from 19 to 74 days (Bonnet
97 et al., 2017; Rudorff et al., 2014a). In Lake Calado, local runoff represents the dominant source
98 of water input with 57% (Lesack & Melack, 1995), so that the maximum volume of river water
99 in the lake occurs before the river flood due to local contributions from the basin in this period
100 (Ji et al., 2019). On the other hand, the main water input comes from the river in Lago Grande de
101 Curuai and Lago Janauacá, representing, respectively, 77% (Bonnet et al., 2008) and 93%
102 (Bonnet et al., 2017) of the total water sources. Rudorff et al. (2014b) showed that overbank flow
103 in the Curuai floodplain accounts for 93% of the total flow in the river-floodplain direction and
104 54% of the flow in the opposite direction (floodplain-river), with the remaining flow being
105 channelized. These lakes illustrate the heterogeneity in river-floodplain hydrodynamics in
106 Amazon floodplain systems. Moreover, water fluxes in these systems were not described in most
107 studies. The first (and only, to our knowledge) validation of water velocity in an Amazonian
108 floodplain was performed by Pinel et al. (2019) for Lake Janauacá. Therefore, there is still a gap
109 in knowledge about the understanding of this complex and important systems.

110 The accuracy of the models used to understand the detailed hydrodynamics of the
111 floodplain over an extensive region is limited by the topographic data. On the one hand, accuracy
112 is limited by the quality and resolution of global DEMs in regional applications, and on the other
113 hand, the study area is limited by in situ bathymetry, as in local models. To overcome this
114 limitation, Fassoni-Andrade et al. (2020a) estimated the topography of a large reach of the
115 Amazon River floodplain (~40,000 km²) at 30 m resolution using remote sensing data. Although
116 topography has not been estimated in permanently flooded areas of channels and lakes in the
117 floodplain, this dataset presents a unique opportunity to investigate the bidirectional flows and
118 the river-floodplain water exchange over a large floodplain area using a two-dimensional
119 hydraulic model with better topographic representation than global DEMs. Therefore, the goal of
120 the present study is to apply a hydraulic model in the central floodplain Amazon using this
121 dataset, in order to describe the floodplains hydrodynamics of hydrological years characterized
122 as normal (2008), intense (2009), and weak (2010) flood conditions.

123 The study is divided into methodology (Section 2), validation (Section 3), results (Section
124 4), and conclusions (Section 5). At the beginning of sections 3 and 4 we synthesize in topics the
125 lessons learned about the modeling and the system hydrodynamics to highlight the main results.

127 2. Data sets and methods

128 2.1. Hydraulic model and simulation domain

129 Recent advances from the HEC-RAS model allows the representation of two-dimensional
130 flows from the numerical solution of the shallow water equations. It represents the inertia terms,
131 pressure gradient and gravitational effects, friction, turbulence, and Coriolis effects. Details of
132 the formulations and numerical schemes used in the model (6.0.1 version) can be found in
133 Brunner (2016).

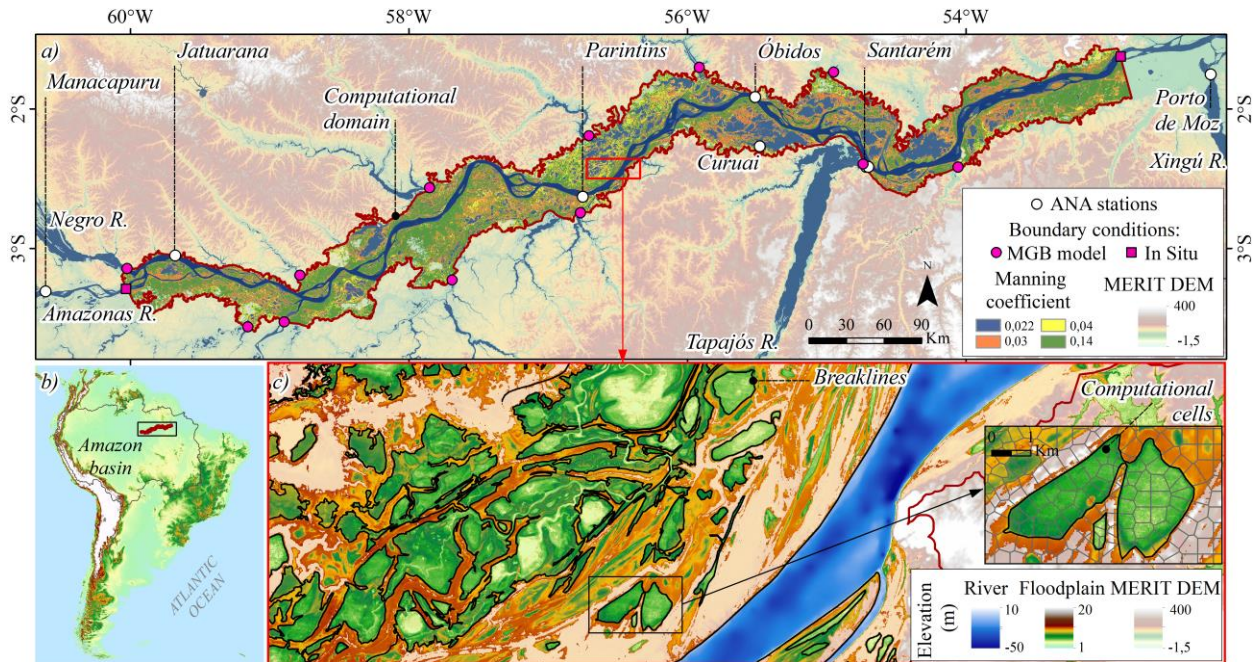
134 The model was applied to 1100 km reach of the Amazon River between the confluence of
135 the Negro and Xingu rivers, where an extensive floodplain is present (Figure 1). The
136 computational domain, which covers ~40,000 km², was delimited from a 1 km buffer of the
137 Amazon wetlands mask (Hess et al., 2015; Figure 1).

138 The simulation covered 3 hydrological years (November 2007 to October 2010), that
139 comprises normal (mid-2008), intense (mid-2009) and weak (mid-2010) flood conditions
140 (Filizola et al., 2014). An initial period of 5 months was considered as model initialization,
141 allowing the filling of the floodplain before the evaluated period.

142 The time series of Amazon discharge from the Manacapuru station, located ~67 km
143 upstream of the domain upstream limit (Figure 1), was used as a boundary condition of the
144 Amazon River. Detailed information for this and other stations operated by the Agência Nacional
145 de Águas e Saneamento Básico (ANA; snirh.gov.br/hidroweb/serieshistoricas) are shown in
146 Table S1 in supporting information. Downstream, water level time series from the Porto de Moz
147 station (operated by ANA) was used, which represents the water level of the Xingu River at its
148 confluence with the Amazon River, located ~77 km downstream from the domain (Figure 1).
149 Due to the backwater effect on the Amazon River tributaries, the station can be representative of
150 the Amazon River level. The vertical levelling of this station (EGM 2008) was done considering
151 the altimetry level at a nearby virtual station of Sentinel-3A satellite (station
152 amz_amz_s3a_0433_01; hydroweb.theia-land.fr/) with an estimated bias of 1.108 m (49 data).
153 Tidal effect from water level was filtered using a moving window of 28 days.

154 The discharges of the main tributaries in the domain were considered as boundary
155 conditions from simulated data performed by Siqueira et al. (2018) using the MGB hydrological
156 model (Collischonn et al., 2007). For this, 12 tributaries that intersect with the computational
157 domain were selected as they represent up to 99% of the average modeled flow contributing to
158 the computational domain (see Figure 1).

159



160

161 Figure 1. a) Location of computational domain ($\sim 40,000 \text{ km}^2$), boundary conditions and ANA
 162 stations. Manning coefficient mapping (within boundary) and topographic model MERIT DEM
 163 (outside boundary). b) Location of the central region of the Amazon basin. c) Detail of the
 164 floodplain topography, position of computational cells and breaklines used in the model.

165

166 2.2. Topography and computational mesh

167 A composite topography map was produced by merging several databases. In the
 168 Amazon River and open water areas of the floodplain, the topography estimated by Fassoni-
 169 Andrade et al. (2020a) at 30 m spatial resolution was used (Figure 1a; available at
 170 data.mendeley.com/datasets/vn599y9szb/1). This mapping was created by digitizing nautical
 171 charts for the rivers, and using the Flood2Topo method (Fassoni-Andrade et al., 2020b) via
 172 optical satellite data representing the topographic variation of lakes and narrow channels in the
 173 open water regions of the floodplain. Validation using locally derived bathymetry showed a root
 174 mean square error (RMSE) of 90 cm for the floodplain bottom level. However, the bathymetry of
 175 deeper regions in the floodplain, which are always flooded, is underestimated since it represents
 176 the lowest observed water level in 30 years. The average bias of the river bathymetry,
 177 documented as 5 m (Fassoni-Andrade et al., 2020a), was discounted in the elevation values.

178 In the flooded vegetation and upland areas, topography was obtained using MERIT DEM
 179 v1.0.1 (Multi-Error-Removed Improved-Terrain DEM; available at [hydro.iis.u-
 180 tokyo.ac.jp/~yamada/MERIT_DEM/](http://hydro.iis.u-tokyo.ac.jp/~yamada/MERIT_DEM/)). This terrain elevation model was chosen because it has
 181 global coverage and comprises a removal of absolute bias, noise, and vegetation height from
 182 SRTM3 DEM and AW3D-30m v1 data (Yamazaki et al., 2017). The vertical reference of the
 183 model (EGM 1996) was adjusted to the EGM 2008 model using the MSP program GEOTRANS
 184 3.7 (available at: earth-info.nga.mil/GandG/geotrans/index.html#zza1).

185 HEC-RAS model uses an unstructured computational mesh in which the orientation and
 186 size of the cells can vary according to topographic variation, so that breaklines can be included to

187 define the orientation of the computational cell faces. Thus, breaklines were added (e.g., Figure
188 1d) considering a manual digitization of the topographic contours of the river banks and in
189 floodplain based on the isolines formed by the 90% and 60% flood frequency of the flood
190 frequency map elaborated by Fassoni-Andrade et al. (2020a). These thresholds (90% and 60%)
191 roughly delineate the location of greater topographic variations, such as riverbanks. The
192 computational mesh generated with a nominal cell size of 400 m (detailed representation through
193 breaklines in smaller features) resulted in ~260,000 cells. Despite the nominal size of 400 m,
194 smaller features were represented through the breaklines considering the 30 m topography.

195

196 **2.3. Manning's roughness coefficient**

197 Manning's roughness coefficient map in the floodplain (Figure 1) was prepared based on
198 the Amazon wetland land cover mapping of Hess et al. (2015). Manning's values were assigned
199 for each class based on recommendations by Arcement Jr.; Schneider (1989) e Chow (1959),
200 according to Table S2. More bathymetry, water velocity and level data in the floodplain would
201 be needed for manning calibration in the floodplain, with possibly weak impacts on the
202 quantitative conclusions of this study.

203 Manning's value in the Amazon River was calibrated for the period from September 1,
204 2006, to August 31, 2007 (1 year). The lowest RMSE of the water level simulated and observed
205 at the stations at Jatuarana (0.19 m), Parintins (0.13 m) and Santarém (0.21 m; ANA operated
206 stations; Location in Figure 1) resulted from a Manning coefficient of 0.022. Lefavour and
207 Alsdorf (2005) assumed a Manning coefficient of 0.025 with an error of 12% for discharge
208 estimation in the Solimões River considering a sand channel without vegetation. Wilson et al.,
209 (2007) calibrated a regional hydraulic model of the lower Solimões River using values in the
210 range between 0.022 and 0.028 based on the estimation of Lefavour and Alsdorf (2005).
211 Therefore, although the value found is low compared to values of Rudorff et al. (2014a; 0.031)
212 and Trigg et al. (2009; 0.032) it is within the uncertainty bound considered by Lefavour and
213 Alsdorf (2005).

214

215 **2.4. Modelling performance metrics**

216 The hydrodynamic model was validated against in situ and satellite observations to
217 access its capability to represent the flooded areas, water surface elevation and water flows in
218 river and floodplains.

219 Several remote sensing-derived Amazon flood extent databases have been developed in
220 recent years to characterize flooding in Amazon (Fassoni-Andrade et al., 2021). This is not a
221 trivial mapping and the different approaches have led to disagreements, as shown by the
222 comparison documented in Fleischmann et al. (2022). We used two basin-scale databases that
223 consider periods of maximum and minimum inundation (Hess et al., 2015; Rosenqvist et al.,
224 2020). The Hess mapping (hereafter called HESS) (Hess et al., 2015), one of the most widely
225 used in the validation of hydrologic-hydrodynamic models in the Amazon basin, depicts wetland
226 inundation and vegetation for the central Amazon basin based on JERS SAR imagery for the
227 flood and low-water periods - May 1996 and October 1995 (available at
228 https://daac.ornl.gov/LBA/guides/LC07_Amazon_Wetlands.html). Rosenqvist's mapping
229 (hereafter called ALOS) (Rosenqvist et al., 2020), on the other hand, considers the maximum and

230 minimum flooding of 3 most recent hydrological years derived from the ALOS-2 SAR data:
 231 2014-2015, 2015-2016 and 2015-2017 with 50 m spatial resolution (available at
 232 <https://www.mdpi.com/2072-4292/12/8/1326>). These mappings do not correspond to the
 233 simulation period (2006-2010), so three simulated periods of low water (November 1, 2007,
 234 2008, and 2009) and high water (May 1, 2008, 2009, and 2010) were compared with these
 235 mappings. For this purpose, the fit metric (F , Equation 1) was used to determine the accuracy of
 236 the model (Schumann et al., 2009).

$$237 \quad F = \left(\frac{a}{a+b+c} \right) 100 \quad (1)$$

238
 239 where a represents the total inundated area correctly mapped by the model, b is the inundated
 240 area not mapped by the model (underestimate), and c is the area not inundated and mapped by
 241 the model (overestimate).

242 The water surface elevation records observed in situ at Óbidos and Curuai stations were
 243 considered for model validation (ANA operated stations; Location in Figure 1). In addition,
 244 satellite altimetry data from virtual stations spread along the river from the JASON2/JASON3
 245 and ENVISAT satellites were also considered. These virtual stations are located at intersections
 246 of the altimeter track with the river and are available at hydroweb.theia-land.fr (Silva et al.,
 247 2010). Information for these stations can be found in Table S1. The metrics evaluated were: i)
 248 RMSE, ii) Bias, iii) Pearson correlation coefficient (r), and vi) Nash-Sutcliffe efficiency
 249 coefficient (NSE).

250 Finally, the water flow of the Amazon River was evaluated at Óbidos (the lowermost
 251 hydrological gauge station in the Amazon basin) and at the Curuai floodplain. The Óbidos
 252 station continuously provides water level data and some flow measurements, in addition to the
 253 rating curve. Since no flow was measured between 2006 and 2010 at Óbidos, we used the rating
 254 curve for model validation, which may have large uncertainties (Filizola et al., 2014). In
 255 addition, we were able to obtain flow measurements in the Curuai floodplain during the 2006
 256 flood season using a SonTek 1.5 MHz Mini Acoustic Doppler Current Profiler (ADCP) with
 257 errors smaller than 3%. Moving boat measurements were carried out with the Mini ADCP
 258 assembled on a home-built Catamaran platform integrated with a GPS. The ADCP platform was
 259 placed on the left side of the boat, near the bow, to avoid interference from the boat engine on
 260 measurements. The boat speed ranged from approximately 0.05 to 0.2 m s⁻¹. The same metrics
 261 for the water level were considered to evaluate the water flow.

262

263 **3. Validation**

264 **3.1. Flood extent**

265 *Modelling lessons: 2D high resolution model improved the representation of flood extent*
 266 *compared to past modelling studies in the Amazon. Model accuracy for flood extent is usually*
 267 *better at high water than low water. Errors may be related to topography, local precipitation*
 268 *and evapotranspiration, and uncertainty of remote sensing maps.*

269

270 Table 1 shows the total flood extent area mapped for the ALOS and HESS products. The
 271 area estimated by the ALOS product is 30 to 50% smaller than the area from HESS product. The
 272 interannual variability of the flood extent from the ALOS product hardly shows any difference
 273 between the years 2014 and 2017 (Table 1).

274 Table 1 also presents the fit metric used to compare the simulations considering low and
 275 high water periods for the three years simulated. The model performance was higher during the
 276 high water period (up to 60%) compared to the low water period (~50%). Although the metrics
 277 for both products are similar at low water, there are many more areas of simulated
 278 overestimation with the ALOS product compared to the HESS product (see green areas in Figure
 279 2a). This is similar during the high water period (see green areas in Figure 2b), when the metrics
 280 for the HESS product (81-82%) are better compared to the ALOS product (56-58%). There is no
 281 significant variability in the metrics among the years evaluated indicating that the discordance
 282 between the simulated years (2007-2010) and the years of observations (1995-1996 and 2014-
 283 2017) is not as significant for validation as the product considered.

284 Applications of hydrodynamic models to Amazon floodplains at different scales found fit
 285 metric values ranging from 23 to 51% (low water) and 70 to 81% (high water) compared to
 286 HESS mapping. Paiva et al. (2013) represented the extent of large-scale flooding in the Amazon
 287 basin from the MGB model with values of 34% at low water and 70% at high water. Wilson et
 288 al. (2007) and Rudorff et al. (2014b), in regional applications of the LISFLOOD-FP 2D model
 289 along the Amazon River reaches, found values of 23 and 51% at low water and 72 and 81% at
 290 high water, respectively. Therefore, our model represented the flood extent relatively well, with
 291 average F values of 52% in the low water period and 81-82% in the high water period against
 292 HESS product. In addition, the accuracy is of local relevance ($F > 0.65$) according to the criteria
 293 established by Fleischmann et al. (2019).

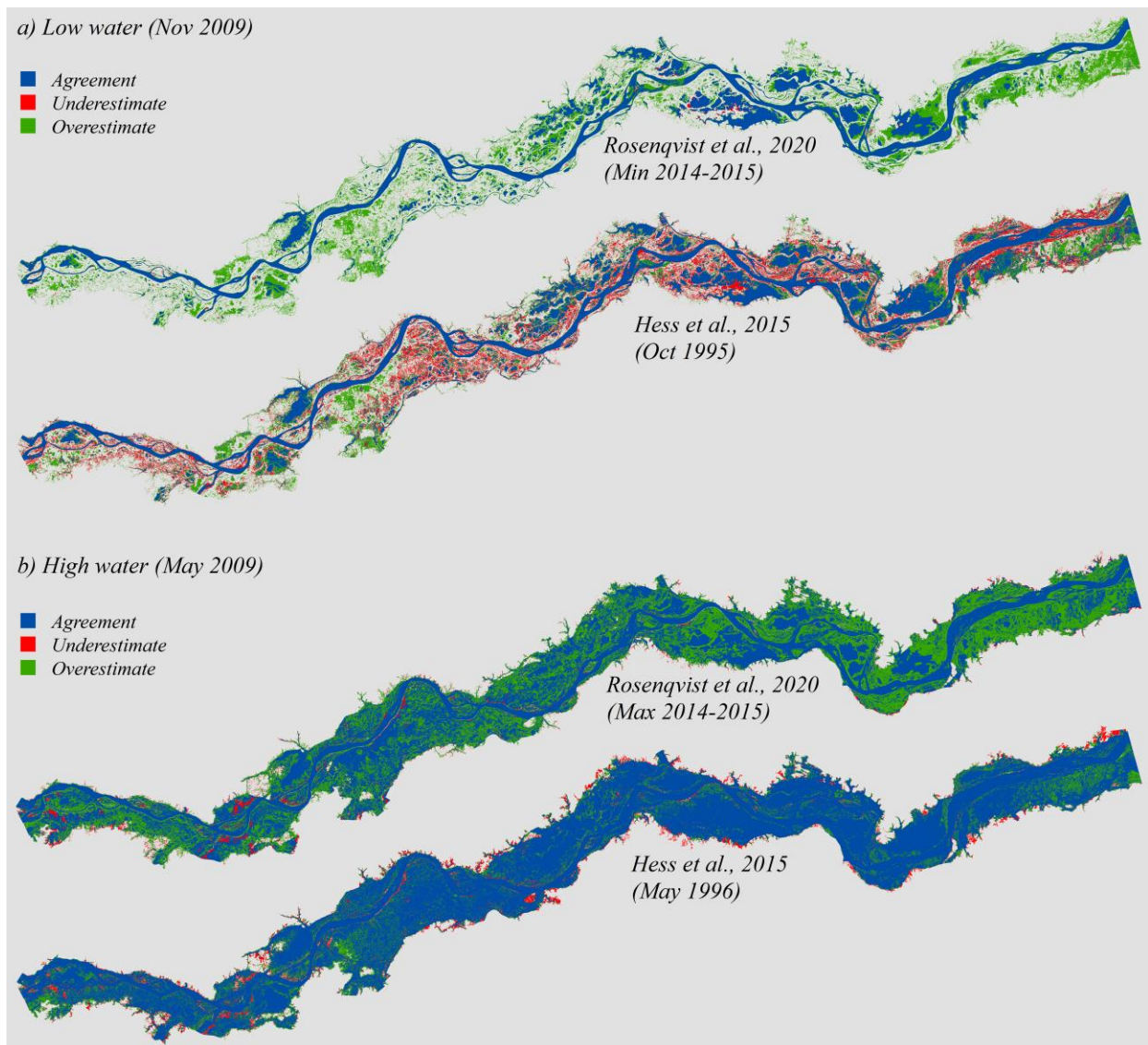
294 Errors in topographic mapping and the lack of representation of processes such as local
 295 precipitation and evapotranspiration in the floodplain can be sources of uncertainties in the flood
 296 extent mapping by the hydrodynamic model, especially in the low water period. However, it is
 297 noteworthy that the various remote sensing-derived water extent databases also have large
 298 inconsistencies among them. For example, Fleischmann et al. (2022) showed that HESS and
 299 ALOS mapping tend to underestimate the maximum inundation compared to subregional remote
 300 sensing-derived products, and there are large differences in minimum inundation among the
 301 different products.

302

303 Table 1. Fit metric for HESS and ALOS products considering the low and high water periods

	Low water (November)				High water (May)			
	Flooded area	F 2007	F 2008	F 2009	Flooded area	F 2008	F 2009	F 2010
HESS	17942.38 km ²	52%	52%	52%	31277.83 km ²	81%	82%	81%
ALOS 2014-2015	8938.60 km ²	51%	50%	48%	21760.10 km ²	58%	59%	58%
ALOS 2015-2016	8130.33 km ²	46%	45%	44%	20130.50 km ²	56%	56%	56%
ALOS 2016-2017	8641.35 km ²	49%	48%	47%	20679.30 km ²	56%	56%	56%

304



305

306 Figure 2. Flood extent mapped by the model and remote sensing products (blue), flood extent not
 307 mapped by the model (underestimate), and flood extent mapped only by the model
 308 (overestimate) considering ALOS and HESS products and simulated in November (a) and May
 309 (b) of 2009.

310

311 3.2. Water surface elevation

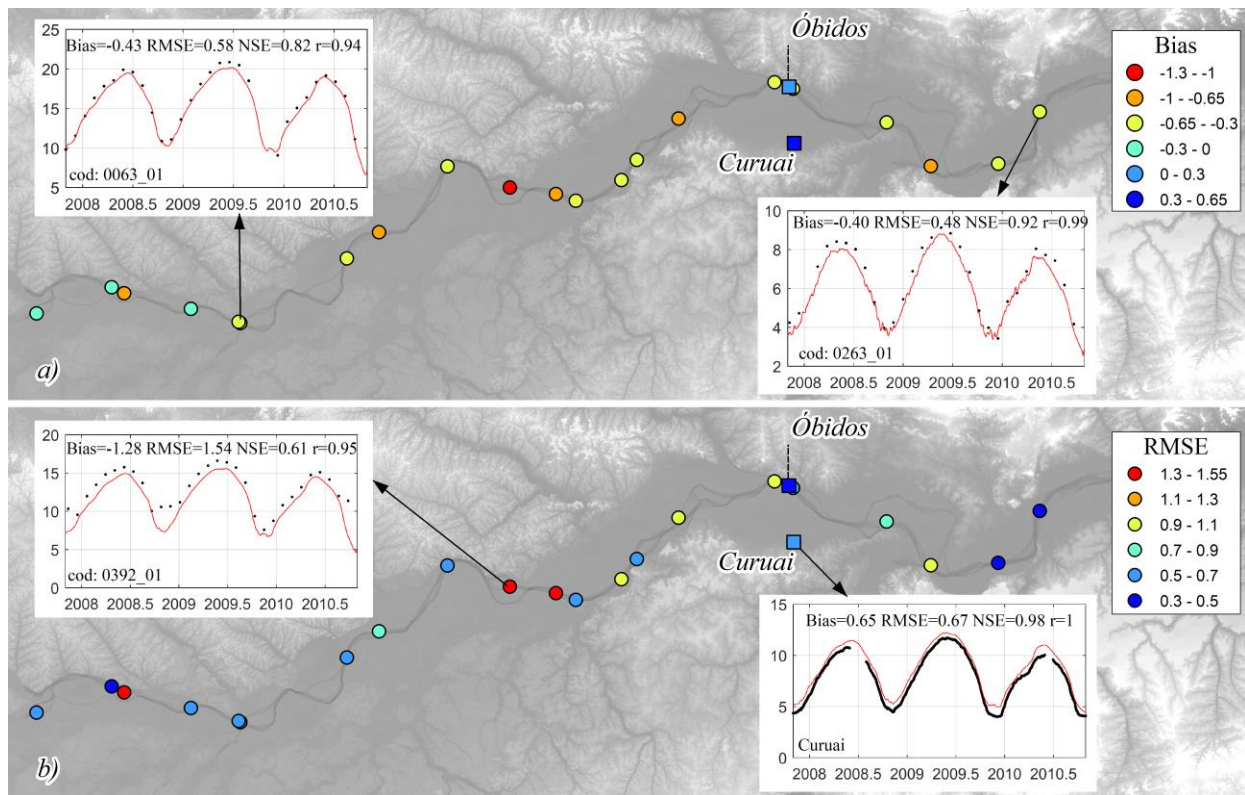
312 *Modelling lessons: 2D high resolution model improves the representation of water*
 313 *surface elevation of the Amazon flood wave compared to past modelling studies. Error is small*
 314 *compared to the flood amplitude.*

315 Absolute water surface elevation in the river was well represented in the 23 stations
 316 evaluated (Table S3), with an average bias of -0.45 m, an RMSE of 0.77 m, an NSE of 0.87, and
 317 an r of 0.98 (values considering the EGM 2008 model). The bias and RMSE of each station are

318 shown in Figure 3. Only the stations monitored by ANA agency showed a positive bias (Óbidos
 319 and Curuai), while the altimetry stations consistently showed a negative bias. The highest RMSE
 320 (1.54 m) was observed at a station located in a channel with underestimation in the low water
 321 period, as presented in Figure3b (Station 0392_01).

322 The errors are small in relation to the annual flood amplitude (4 to 10 m; Station 0063_01
 323 and 0263_01 in Figure 3a) and compared to the errors found by Wilson et al. (2007), which
 324 obtained an RMSE of 0.99 m at flood and 3.17 m at low water in the Amazon River. On the
 325 other hand, Rudorff et al. (2014b) found errors of 0.27 m at the Curuai station, considering the
 326 local hydrodynamic simulation of this floodplain using observed bathymetry. Our results also
 327 have a better agreement with observations compared to large-scale modeling in the Amazon
 328 basin. For instance Paiva et al. (2013) obtained a NSE of 0.2-0.4 at Óbidos and Yamazaki, Lee,
 329 et al. (2012) obtained a NSE of 0.7 at Óbidos, where water surface elevation anomalies were
 330 evaluated.

331



332

333 Figure 3. Validation of absolute water surface elevation derived from the model against in-situ
 334 observations of gauging stations (squares) and satellite altimetry data (circles). Spatial
 335 distribution of model performance statistics: Bias (a) and RMSE (b). Time series of the model
 336 (red line) and observed (black dots) water elevation.

337

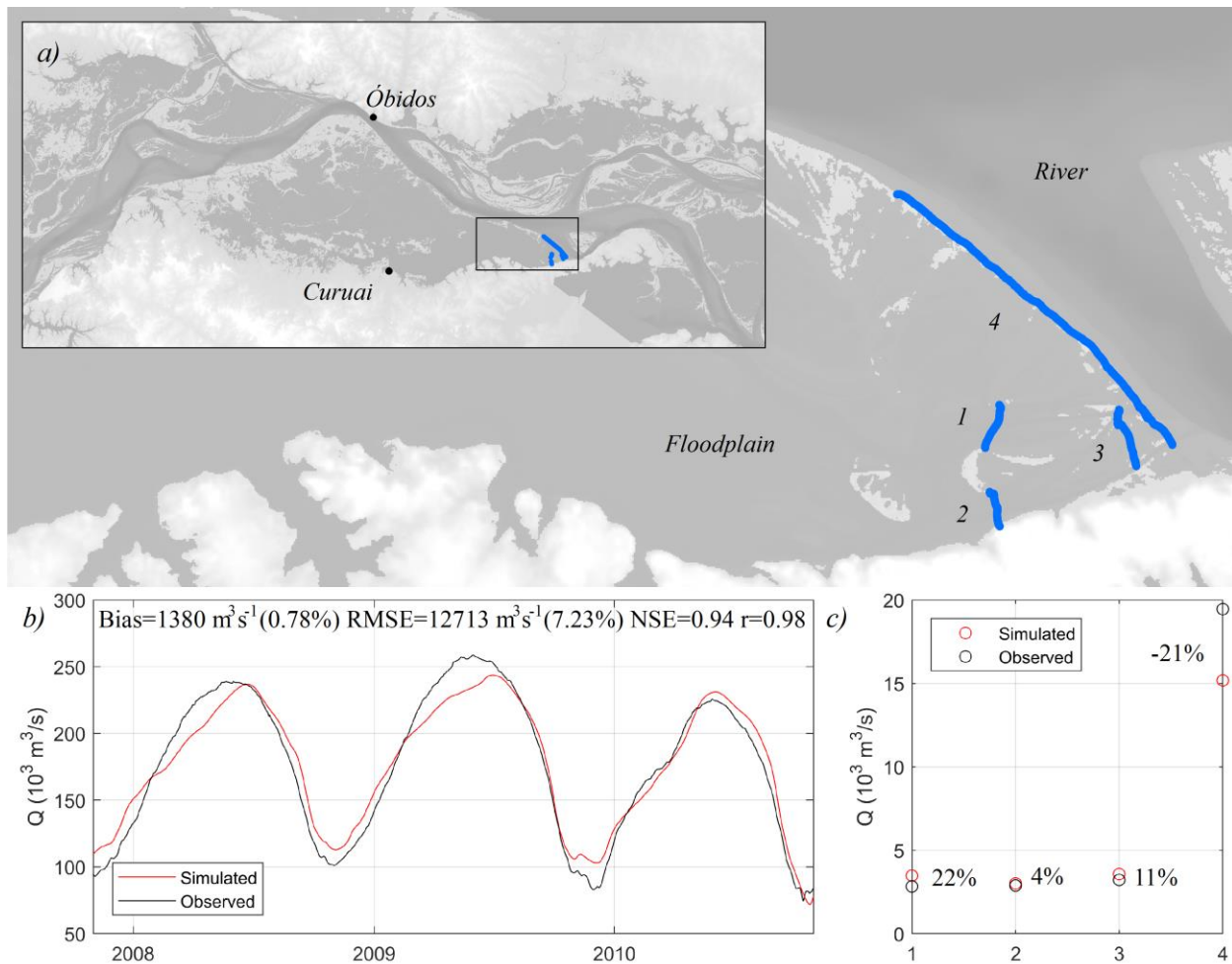
338 3.3. River and floodplain flow

339 *Modelling lessons: 2D high resolution model provides accurate representation of*
340 *Amazon River discharge. Appropriate representation of expressive floodplain flow with errors*
341 *smaller than 20%.*

342 The Amazon River discharge at Óbidos station was adequately represented by the model
343 with a positive bias of $1380 \text{ m}^3\text{s}^{-1}$ (0.78% of the mean observed discharge) and an RMSE of
344 $12713 \text{ m}^3\text{s}^{-1}$ (7.23% of the mean observed discharge) and relatively high $\text{NSE} = 0.94$. The values
345 during the rising period (February to June) were underestimated, while during the rest of the year
346 discharge values were slightly overestimated (Figure 4a). It is likely that this underestimation is
347 related to the uncertainties of the rating curve at Óbidos since it is calculated considering a single
348 stage-discharge relationship. As Filizola et al. (2014) pointed out, a large amount of water goes
349 to the floodplain during the flood, so the stage-discharge relationship may be different in this
350 period compared to the low water period.

351 The observed flow was also evaluated across four transects located at the downstream
352 outlet of the floodplain on June 26, 2006 (blue spots profiles in Figure 4b and c). In spite of the
353 uncertainty of the bathymetry used in the simulation, the model adequately represented the flows
354 on the floodplain, with differences from the observed flow ranging from -21% to 22% ($(Q_{mod} -$
355 $Q_{obs})/Q_{mod}$). The flows in the three main channels (profiles 1, 2, and 3) were overestimated,
356 while the flow in the longest profile was underestimated (profile 4). What is noteworthy about
357 these measurements is the order of magnitude of the flows (ranging from $3'000$ to $19'000 \text{ m}^3\text{s}^{-1}$).
358 The outflow on the floodplain in profile 4 represents 8.3% of the discharge observed at Óbidos
359 on the same day ($234'000 \text{ m}^3\text{s}^{-1}$) and is greater than the average discharge of the Tapajós River
360 ($14'500 \text{ m}^3\text{s}^{-1}$).

361



362

363 Figure 4. Validation of water flow derived from the model (red line/dot) against observation
 364 (black line/dot) at Óbidos station (a) and in the floodplain on June 26, 2006 (b and c). Blue spots
 365 indicate location of ADCP profiles (1, 2, 3, and 4).

366

367 4. Flood dynamics on the floodplain

368 4.1. Volume, depth, and flood extent

369 *Lesson 1: Annual volume variation of 160 km^3 in the central Amazon floodplain.*
 370 *Variation represents about 3% of the Amazon River volume exported to the ocean annually.*
 371 *Intense and weak floods cause interannual variability of 20% in volume variation.*

372 *Lesson 2: Average water depth in the central Amazon floodplain ranges from 2.5 to 7.1 m*
 373 *annually. Intense and weak floods cause variations of up to 1 m at high water or 22% of the*
 374 *annual variation.*

375 *Lesson 3: Annual flood extent variation of $7'560 \text{ km}^2$ in the central Amazon floodplain.*
 376 *Intense and weak floods cause interannual variability of only 3% in flood extent variation. Flood*
 377 *extent finds a plateau in extreme floods, possibly due to topographic constrains.*

378 *Lesson 4: Significant flood extent and volume hysteresis that may be related to the*
 379 *floodplain hydrodynamic complexity.*

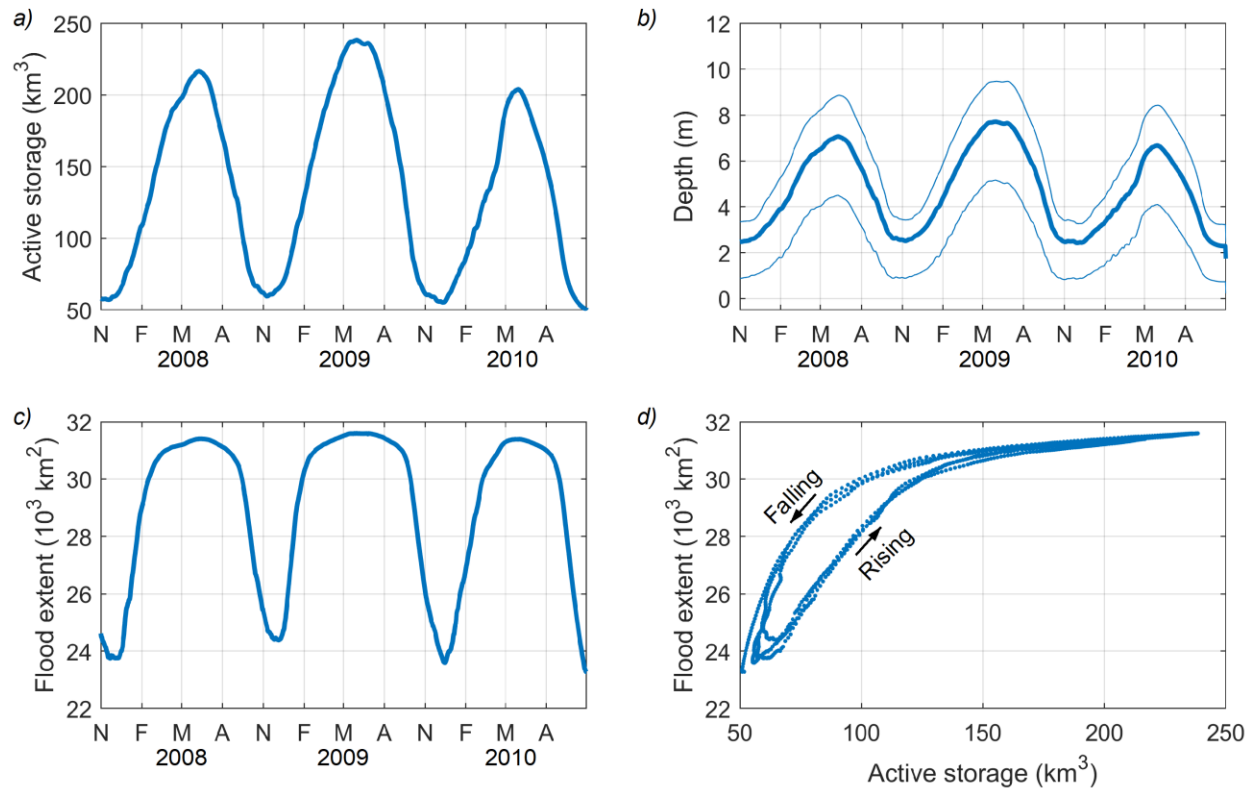
380 The active volume stored during 2007 and 2010 in the floodplain is presented in Figure
381 5a. In the low water period (November), the volume stored ranged from 55.3 km³ (2010) to
382 59.68 km³ (2009), while in the high water period (June), the volume stored ranged from 204 km³
383 (2010) to 238 km³ (2009). Therefore, the floodplain has an average volume variation of 162 km³,
384 i.e., annually, this volume is stored and drained in the floodplain between low water and flood
385 periods. The volume stored annually in the central Amazon floodplain (162 km³) represents
386 about 2.8% of the Amazon River volume exported to the ocean annually. This annual variation is
387 larger than the estimated over the open-water floodplains of the central Amazon (116 km³;
388 Fassoni-Andrade et al., 2020a) and smaller than the estimate over the Amazon floodplains in six
389 square regions of 330 km × 330 km (285 km³; Alsdorf et al., 2010). It represents 13.5% (Papa et
390 al., 2013) to 18% (Frappart et al., 2019) of the total surface water storage at the Amazon basin
391 scale estimated by remote sensing data. Furthermore, the estimated volume stored in the
392 floodplain showed a difference of 34 km³ at the flood peak between years characterized by
393 intense (2009) and weak (2010) flood. This volume is significant and represents 20% of the
394 annual volume variation and 60% of the average volume stored in the floodplain during the low
395 water period.

396 The water depth in the floodplain showed a similar pattern to that of the stored volume
397 (Figure 5b), with an average depth of 4.62 m, i.e., the average depth ranges from 2.5 m to 7.12 m
398 between the low water and high water periods. The average depth variation in the flood period
399 was 40 cm lower in the dry year (2010) and 60 cm higher in the wet year (2009) compared to a
400 normal year (2008). These values can be significant when considering the amplitude of the water
401 level, which varies from 10 m upstream to 4 m downstream reach (Fassoni-Andrade et al.,
402 2020a). Furthermore, the variation of 1 m between extreme floods (2009 and 2010) represents
403 22% of the annual variation of the average depth.

404 The flood extent showed an average value of 31'500 km² and 23'940 km² during the high
405 water and the low water periods, respectively (Figure 5c), i.e., an annual variation of 7'560 km².
406 These values represent, respectively, 5% and 8% of the mapped wetlands in the Amazon basin
407 during the high and low water periods (Hess et al., 2015). However, in contrast to the strong
408 interannual variation in stored volume, the flood extent presented a plateau during the high water
409 period with differences of ~200 km² between 2009 and 2010, which represents only 2.6% of the
410 average variation between high and low water periods. This means that flood intensity does not
411 have such a large impact on flood extent (2.6%) compared to its impact on volume (20%) and on
412 water depth (22%). The flood extent finds a plateau during the flood possibly due to topographic
413 constrains limited by the geomorphology of the Amazon River and the Uplands (Terras Altas) at
414 the floodplain boundaries

415 The relationship between volume and flood extent on the floodplain indicates a counter-
416 clockwise hysteresis, as also documented by Rudorff et al. (2014b) for Curuai floodplain, i.e., for
417 the same stored volume, the flood extent is larger in the falling than in the rising period (Figure
418 5d). For example, the flood extent was 30'000 m² in the falling period and 28'000 m² in the rising
419 period for a stored volume of 100 km³. This may be related to the floodplain hydrodynamic
420 complexity, as the asymmetry of the Amazon River hydrograph, where the rising period is
421 slower than the falling period (Fleischmann et al., 2016), the reversal of river-floodplain surface
422 water slope (Zhang & Werner, 2015), or the time taken for water to fill deeper parts of the
423 floodplain before flooding upper regions.

424



425
 426 Figure 5. Temporal series of a) active storage, b) average depth \pm 25 and 75 percentile and c)
 427 flood extent in the floodplain. d) The relationship between active storage and flood extent in the
 428 floodplain.

429

430 4.2. River-floodplain flows exchange

431 *Lesson 5: Central Amazon floodplain is fragmented into floodplain units of ~80 km with*
 432 *expressive water inflow/outflow from/to the main river.*

433 *Lesson 6: Extreme floods can offset by one month the timing of the floodplain inflow*
 434 *onset (delay and advance). No interannual variability in the timing of the maximum flood.*

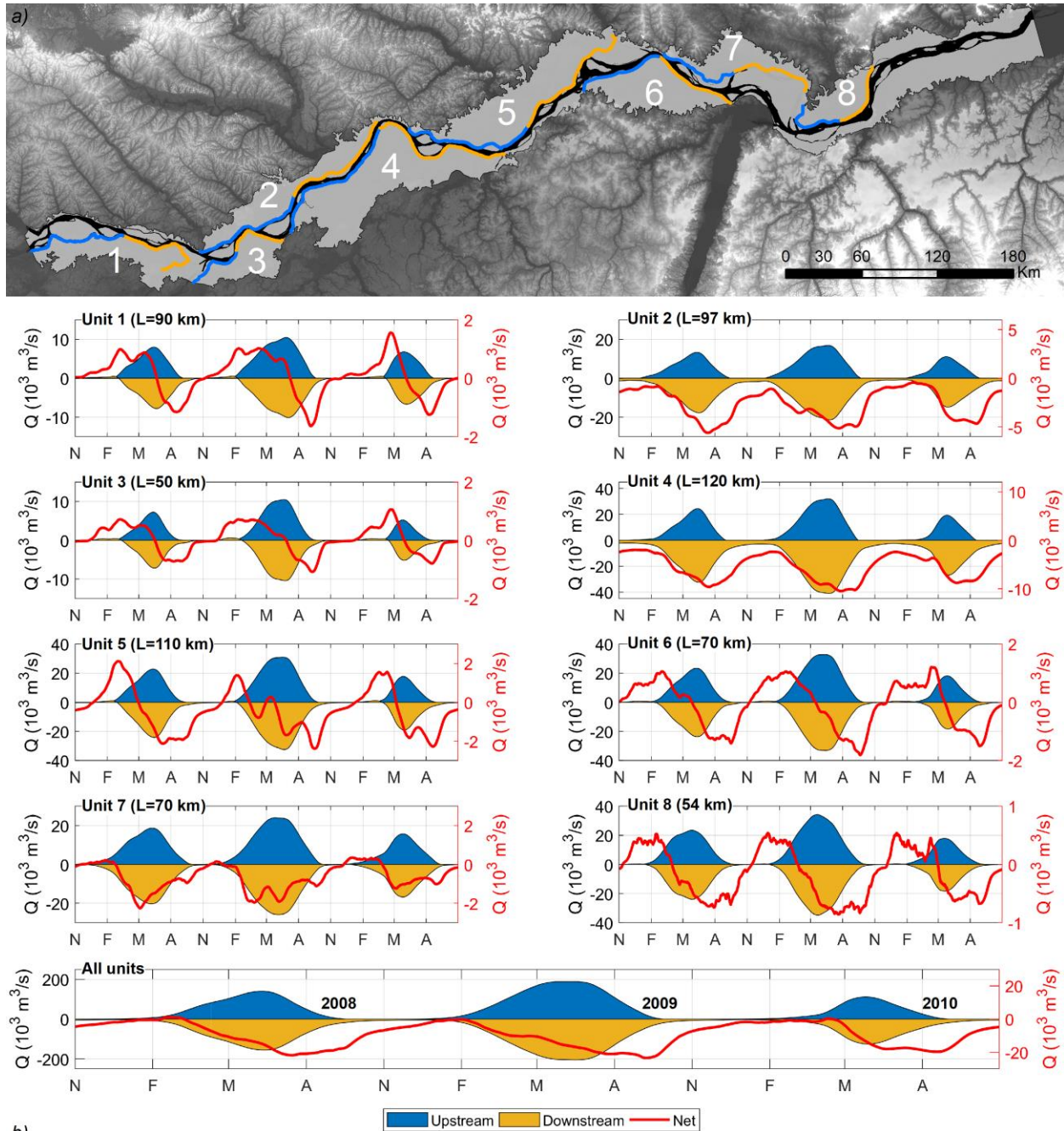
435 *Lesson 7: Gross floodplain inflow and outflow greatly surpass the net inflow and outflow,*
 436 *indicating that the floodplain flux is generally more expressive than storage infilling and*
 437 *outfilling.*

438 *Lesson 8: Variations in flood duration in extreme floods can induce a 33% (22%)*
 439 *increase (decrease) in floodplain inflow.*

440 The water exchange between the Amazon River and the floodplain was evaluated in eight
 441 units by estimating the flow across transects parallel to riverbanks. In each unit, two transects of
 442 equal length (L) were defined: one upstream and one downstream. These transects consider that
 443 most of the water inflow (outflow) in the floodplain occurs in the upstream (downstream) half,
 444 however dominant inflow/outflow boundaries have not been defined. In the Curuai floodplain
 445 (Unit 6), for example, water outflow is predominantly in a smaller downstream transect (Rudorff
 446 et al., 2014a). Figure 6 shows the flows across both transects (blue and yellow), and the resulting

447 net flow (red line). Positive values indicate that the floodplain is receiving water from the river,
 448 and negative values indicate that water is flowing out of the floodplain. Once our model does not
 449 consider infiltration, precipitation, and transpiration processes in the domain, the net flow is the
 450 result of the discharge received from the tributaries.

451



452

453 Figure 6. (a) Map and (b) temporal series of water flow in eight floodplain units from 2008 to
 454 2010. Blue and yellow transects represent, respectively, the upstream and downstream region of

455 each unit (left y-axis), and the red line represents the resulting net flow (right y-axis). Note the
 456 widely different scales in left and right y-axes.

457

458 In all units, the inflow and outflow of water from the floodplain predominates,
 459 respectively, in the upstream and downstream transect, i.e., inflow or outflow can occur in both
 460 transects, but the balance is positive (negative) for the upstream (downstream) transect. In
 461 general, the positive water inflow balance in the floodplain begins with the river flood and
 462 predominates until the flood peak (May/June/July). During the falling period, outflow becomes
 463 predominant with a maximum in August/September, when there is little or no inflow to the
 464 floodplain. Negative balance (floodplain flow into the river) continues to occur in the units with
 465 small values until the onset of the flood. However, in regions 2 and 4, this flow from the
 466 floodplain to the river is greater in the low water period because there is a significant flow
 467 contribution from the tributaries.

468 In units 1, 3, 5, and 6, flooding begins between February and April, depending on the
 469 year: March in 2008, February in 2009, and April in 2010. That is, a weak flood and an intense
 470 flood cause, respectively, a delay and an advanced of the water inflow into the floodplain by
 471 approximately one month in these units. These findings are similar to results for Lake Janauacá
 472 in central Amazon (Pinel et al., 2019). Inflow onset in units 2, 4, 7, and 8 occurs in
 473 December/January regardless of the year, therefore, these areas seem to have more connection
 474 with the river from channelized flows. Although the positive balance is initiated in different
 475 months in the units, the maximum inflow and outflow occurs at the time of river peak flood
 476 (June/July), since diffuse overbank throughflow in the floodplain predominates.

477 The water exchange between the river and the floodplain during the flood is very intense
 478 with inflows and outflows ranging from 5'500 to 35'000 m³s⁻¹ (units 3 in 2010 and 8 in 2009,
 479 respectively). However, these values represent the inflow and outflow of water occurring
 480 practically at the same time in the units, i.e., gross floodplain inflow and outflow greatly surpass
 481 the net inflow and outflow, indicating that the floodplain flux is generally more expressive than
 482 storage infilling and outfilling.

483 The total water inflow considering all units (area of 40'000 km²) is maximum during the
 484 2009 flood with values of 189'600 m³s⁻¹, representing more than the flood peak of the Solimões
 485 River in the same year (~160'000 m³s⁻¹). On the other hand, the outflow from the floodplain is
 486 206'000 m³s⁻¹ in the 2009 flood. These values are much lower at the peak of the 2010 weak
 487 flood: the maximum inflow and outflow are respectively to 60% and 62% of the values in 2009.
 488 Therefore, an intense (weak) flood promotes a 33% (22%) increase (decrease) in floodplain
 489 inflow during the flood compared to a more normal year (e.g., 2008, when 142'700 m³s⁻¹ are
 490 seen).

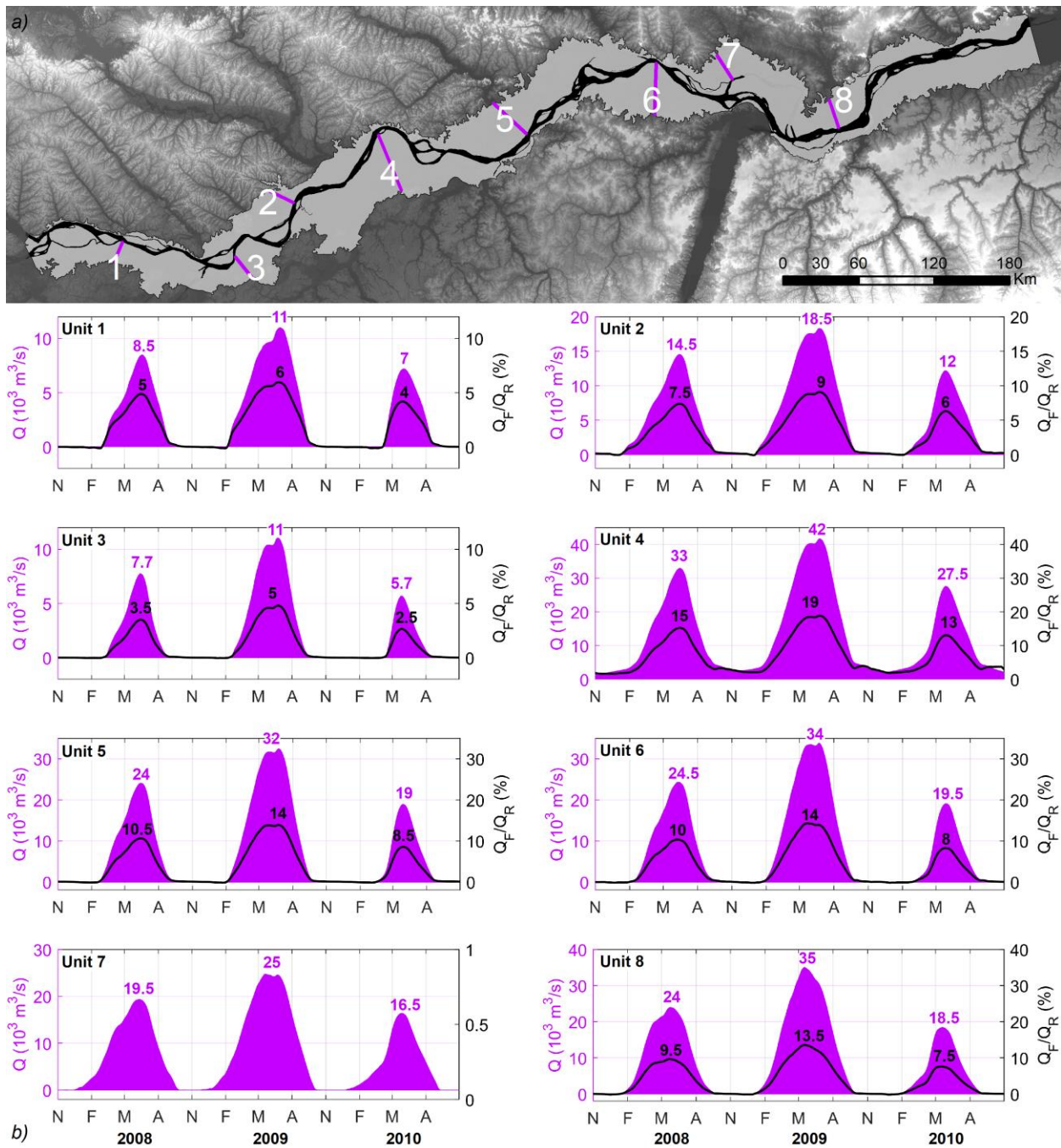
491

492 **4.3. Riverine fluxes over floodplain units**

493 *Lesson 9: Amazon floodplain units work as a river with flows up to 20% of the Amazon*
 494 *River discharge.*

495 *Lesson 10: Heterogeneity in floodplain velocity fields with floodplain channels of active*
 496 *flow and storage areas.*

497 Figure 7 shows the transverse flows across the sections in the floodplain units (purple;
 498 left y-axis) and this flow (Q_F) expressed as a percentage of the Amazon River discharge (Q_R ;
 499 right y-axis) for 2008, 2009, and 2010.



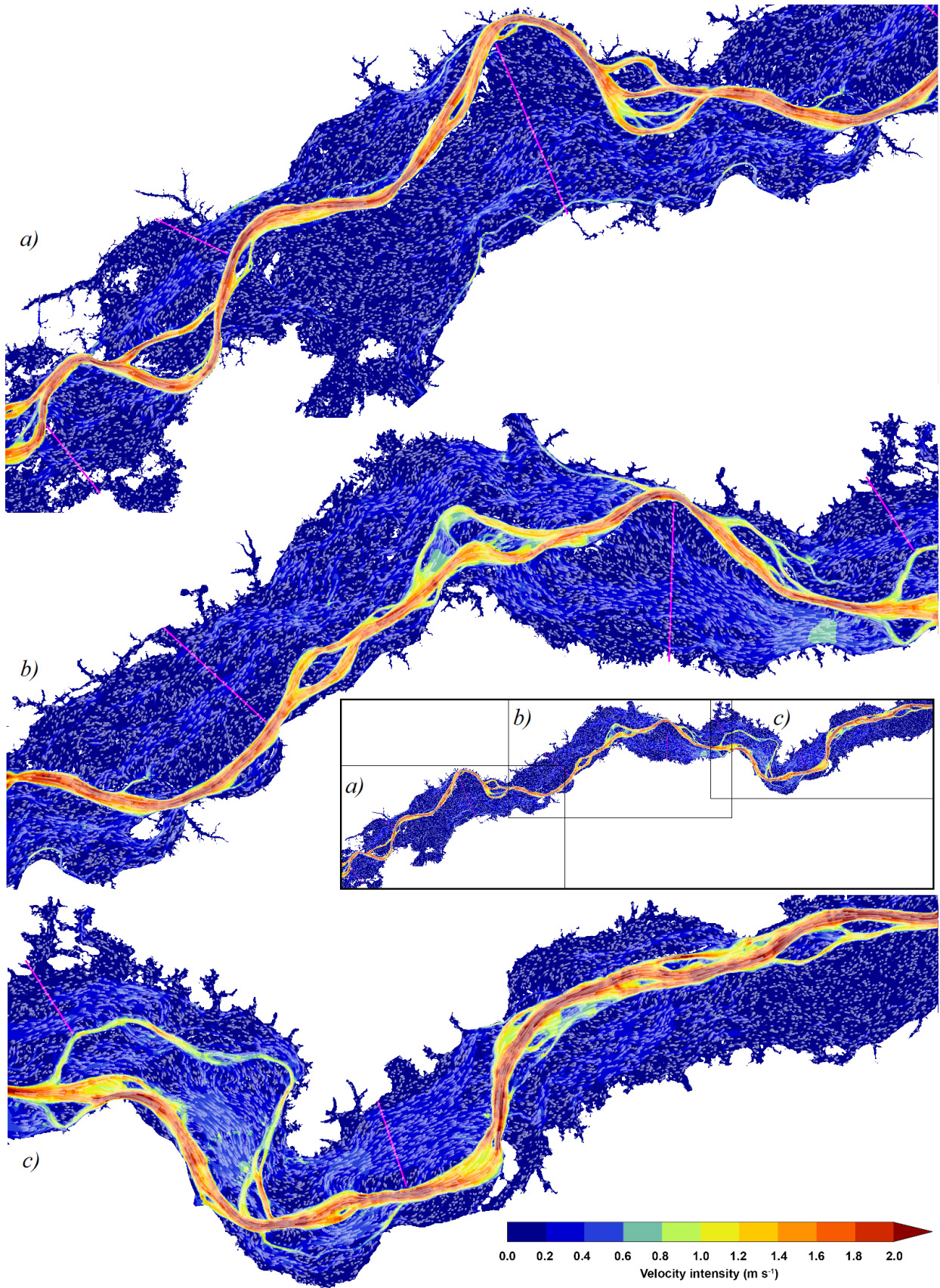
500
 501 Figure 7. (a) Map and (b) temporal series of transverse flows in the floodplain in the eight units
 502 (purple; left y-axis) and the percentage of flow in the transverse transect (Q_F) relative to the river
 503 discharge (Q_R) (black; right y-axis) from 2008 to 2010.

505 Flows along the transverse profiles are towards downstream during the flood (positive
506 values in the graphs) and broadly parallel to the river, as can be seen in Figure 8 for the 2009
507 flood. During 2008 (normal year), floodplain flows vary from 7'700 to 33'000 m³s⁻¹ (units 3 and
508 4) representing from 3.5% to 15% of the Amazon River discharge (average of 8.7%). During
509 intense and weak floods, flows vary from 5% to 19% (2009) and from 2.5% to 13% (2010) of the
510 Amazon River discharge, respectively. These values are very significant, as they are similar in
511 magnitude to the average discharge of the largest tributaries of the Amazon River (e.g., 28'000
512 m³s⁻¹ for the Negro River and 31'000 m³s⁻¹ for the Madeira River). As these flows are not stored
513 in the floodplain (inflow and outflow occur roughly at the same time; Figure 6), the eight units
514 behave as very active zones with riverine fluxes during the flood. Furthermore, the Amazon
515 River can be considered not only as the most voluminous river in the world (Callède et al., 2010)
516 but also as the widest during the flood (ranging from 21 km to 54 km wide), since the floodplain
517 units can be considered as an active extension of the river. Velocity fields (Figure 8) in the
518 floodplain are heterogeneous with storage areas, which may be disconnected from the Amazon
519 River, and active flows in channels.

520 During the low water period, the flow in the cross transects is significantly weaker and
521 may occur in the opposite direction, towards upstream. These reverse flows in February 2009,
522 for example, ranged from 76 m³s⁻¹ to 389 m³s⁻¹ (units 3 and 6). This is also observed in the
523 downstream transects (Figure 6), i.e., there is an inflow in the floodplain in the downstream
524 region during the low-water period, predominantly in February.

525 The estimation of the amount of water exchanged between the Amazon River and the
526 floodplain is not a consensus. From the water balance of six regions along the Amazon River
527 using remote sensing observations, Alsdorf et al. (2010) showed that the filling or drainage of the
528 floodplain accounts for no more than 10% of the river discharge during any time in the regions
529 evaluated. On the other hand, Richey et al. (1989) estimated that up to 30% of the Amazon River
530 discharge is exchanged with the floodplain using water balance and a simplified routing
531 propagation method (Muskingum-Cunge). Getirana et al. (2012) showed much lower values
532 using a global-scale flow routing scheme, with a mean of 2.3% and a maximum of 4% in central
533 Amazon. Our findings showed that from 3.5% to 15% of the Amazon River flow passes through
534 the floodplain during a moderate flood but can reach 20% during an intense flood. Therefore, our
535 results are larger and lower than to Getirana's and Richey's estimates, respectively, however,
536 the two-dimensional hydrodynamic modeling approach performed in this study is the only one
537 that allowed direct estimates of gross floodplain flows.

538



540 Figure 8. Map of water velocity field in the floodplain during the flood period (June 15, 2009).
541 The blue to red colorbar indicates the velocity intensity (m s^{-1}) and the white streamlines the flow
542 direction. The panels are a continuous sequence of the study area, as seen in the inset.

543

544 **4.4. Residence time**

545 *Lesson 11: Water renewal in the floodplain units is high (low) during high water (low*
546 *water) with water residence time around 6 days during high water and several months during*
547 *low water period.*

548 *Lesson 12: Floodplains connectivity increases from upstream to downstream of the*
549 *Amazon River.*

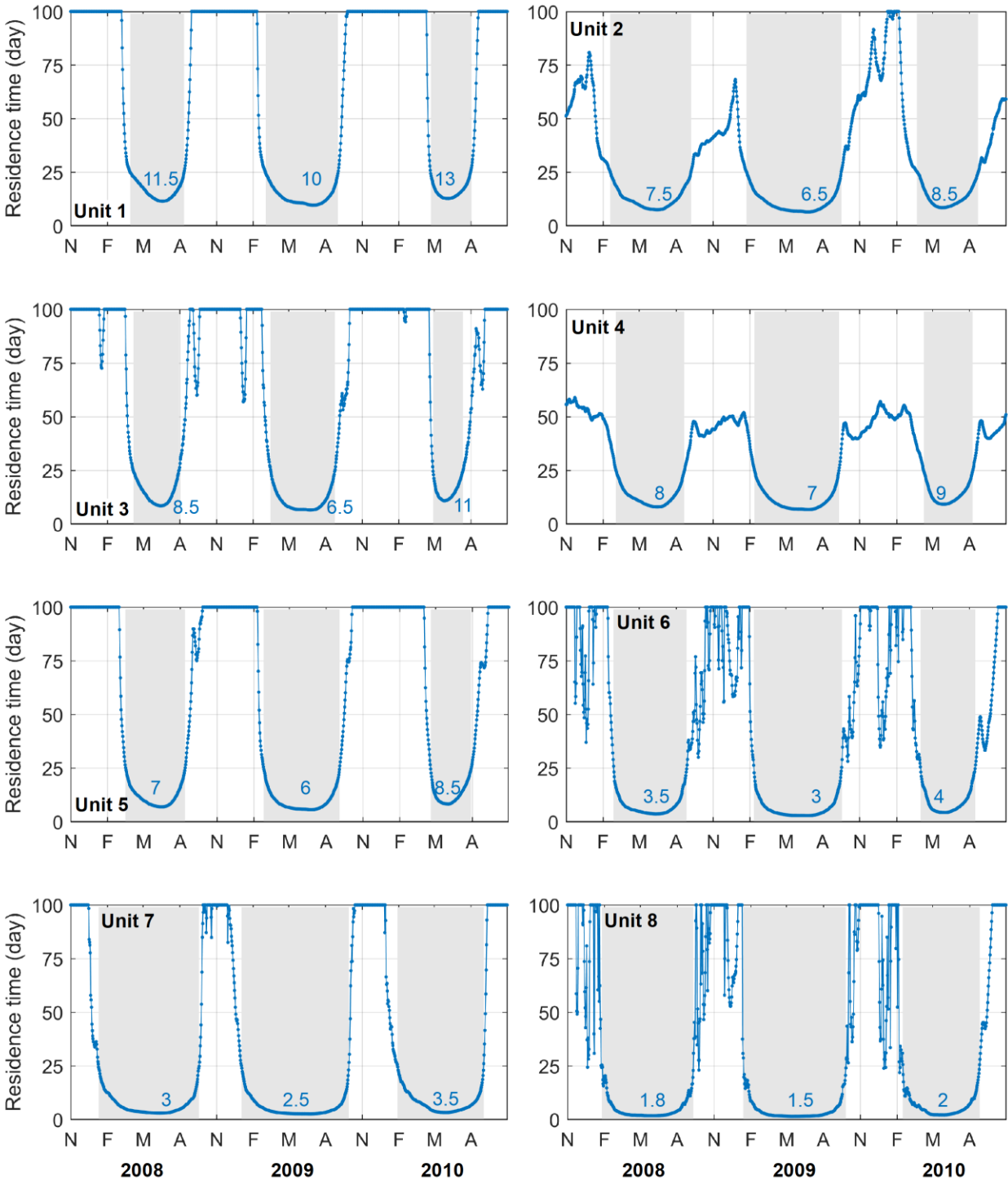
550 *Lesson 13: Intense and weak floods cause variations of up to 80 days in the duration of*
551 *the period of high connectivity.*

552 Water residence time in the floodplain units was calculated by the ratio of water volume
553 to net flow, which represents a condition at a given instant, i.e., high values represent a
554 theoretical steady-state condition that does not actually occur, since the inflows and outflows are
555 dynamic in the floodplain. The residence time can be clearly divided into two periods in the eight
556 units: one of high connectivity of the floodplain with the river during the flood (gray regions in
557 Figure 9) and one of low connectivity during the low water. Water renewal in the flood season
558 (April/May/June) is high with residence time values ranging from 1.5 to 13 days (units 8 and 1,
559 respectively) with an average of 6.4 days for all units. After the flood, residence time increases
560 rapidly in the falling period (August/September/October) to values greater than 100 days at low
561 water (November to January), except for units 2 and 4. In these units, residence time at low water
562 remains shorter, as it varies between 50 and 75 days due to the greater contribution of tributaries.
563 These estimates are global at the scale of the floodplain units, but the residence time may vary
564 within a given floodplain, especially in the low water period, among regions of swift current,
565 such as channels connected to the river, and slower flow regions, such as lakes disconnected
566 from the drainage network.

567 The duration of the high connectivity period, defined here as the period in which the
568 residence time is less than or equal to 25 days (gray regions in the Figure 9), has an average of
569 177 days in all units. In units 1, 3 and 5, the duration of high connectivity varies between 100
570 and 150 days. In units 2, 4 and 6 the duration is 150 to 200 days, and in units 7 and 8 the duration
571 is 200 to 250 days. Therefore, there appears to be an increase in floodplains connectivity from
572 upstream units to downstream units.

573 The mean residence time in 2008 was 6.4 days with the high connectivity period lasting 6
574 months (179 days), whereas in 2009 and 2010, the mean residence time was 5.4 and 7.4 days
575 with high connectivity during 215 and 137 days, respectively. Thus, an intense (weak) flood
576 appears to promote a shorter (longer) average residence time of approximately 1 day and a
577 longer (shorter) high connectivity period between the river and the floodplain of approximately
578 40 days. This is in line with section 4.2, in which an intense (weak) flood causes an advanced (a
579 delay) of the water inflow into the floodplain by approximately one month.

580



581

582 Figure 9. Temporal series of water residence time in the eight units from 2007 to 2010 (restricted
 583 to values smaller than 100days for clarity). Blue labels represent the minimum observed during
 584 the flood and gray regions represent the high connectivity period, defined as the period in which
 585 the residence time is less than or equal to 25 days.

586

587 5. Summary and conclusions

588 In this study, a hydrodynamic simulation of water flows in the central Amazon floodplain
589 was performed for the first time considering a 2D hydrodynamic model and a large area (40'000
590 km²) with detailed topographic information (30 m of spatial resolution). High resolution 2D
591 model improved the representation of water surface elevation of the Amazon River and flood
592 extent in the floodplain compared to past modelling studies. Model accuracy for flood extent is
593 usually better at high water (~80%) than low water (~52%) and the error in water surface
594 elevation (77 cm) is small compared to the Amazon flood amplitude. The model also provides
595 accurate representation of floodplain flow and Amazon River discharge with errors smaller than
596 20%.

597 Part of the modelling errors may be related to topography, local infiltration, precipitation
598 an evaporation, and uncertainty of remote sensing maps (water extent). Despite the small error of
599 the topographic data (90 cm), the permanently flooded areas in the floodplain are underestimated
600 causing uncertainties in these areas in our modeling (depth and volume), especially in the low
601 water period. The representation of hydrological processes in the floodplain can be evaluate in
602 future studies since these processes can affect the residence time and water flow in the floodplain
603 (e.g. Tull et al., 2022).

604 The stored volume, average depth, and flood extent in the floodplain varied on average
605 162 km³, 4.6 m (2.5 to 7.1), and 7'560 km² between the low and high water periods (*Lessons 1,*
606 *2, 3; hereafter L*). The floodplain can be compared with a confined basin in which intense or
607 weak floods, such as that of 2009 and 2010, have more impact on the stored volume and water
608 depth in the floodplain than on the flood extent (*L3*). We observed significant flood extent and
609 volume hysteresis that may relate to in the floodplain hydrodynamic complexity (*L4*).

610 Central Amazon floodplain is fragmented into floodplain units of ~80 km with expressive
611 water inflow/outflow from/to the main river (*L5*). Gross floodplain inflow and outflow greatly
612 surpass the net inflow and outflow, indicating that the floodplain flux is generally more
613 expressive than storage infilling and outfilling (*L7*). Intense and week floods can promote an
614 advance and delay, respectively, of up to one month in the flood onset in some floodplain units,
615 although the peak occurs in the same period of the river flood (May and June; *L6* and *L8*).

616 For the first time, our results show how the Amazon River floodplains are intensely
617 active during the flood (May/June), with parallel riverine fluxes in floodplain units reaching from
618 2.5% to 20% of the main river discharge in the same period (*L9*) and water residence time
619 ranging from 1.5 to 13 days (*L11*). This indicates that the Amazon floodplains work as a river,
620 i.e., the Amazon River is the widest in the world during the flood considering the floodplain (20-
621 50 km wide) as a continuous extension of the river. On the other hand, in the period of low
622 connectivity with the river, the water residence time can be of several months and floodplain
623 flows show negligible values relative to the flood period. The floodplain velocity fields are
624 heterogeneous, with active flow channel and storage areas (*L10*). Furthermore, intense and weak
625 floods promote, respectively, an increase and decrease of the period of high connectivity by 40
626 days due to the advance and delay of water inflow into the floodplain (*L12* and *L13*).

627 This study contributed to understanding of a dynamic and complex system. The 13
628 lessons learned about the Amazon floodplain hydrodynamics open a prospect to explore further
629 questions, such as:

- 630 i) Evaluate and improve rating-curves along the Amazon River, such as in Óbidos,
631 since the floodplain fluxes is not currently considered.
- 632 ii) Understand the effects of intense floods, that have been more frequent in central
633 Amazon (Chevuturi et al., 2022), on riparian communities.
- 634 iii) Improve the representation of hydrodynamic processes in floodplains in large-
635 scale models (e.g. MGB and Camaflood).
- 636 iv) Understand nutrient and sediment variations in the floodplain, since the water
637 mixing strongly influences the biogeochemical characteristics of the water (Wohl,
638 2021).
- 639 v) Estimate gas fluxes in the Amazon floodplain.

640

641 Acknowledgments

642 The authors would like to thank Conrado Rudorff and Walter Collischonn for their insights, and
643 CNPq (Conselho Nacional de Desenvolvimento Científico e Tecnológico) for partially funding
644 this research under the grant numbers 140352/2016-3 (A.C.F.A.). S.W. has been supported by
645 the French AMANECER-MOPGA project funded by ANR and IRD (ref. ANR-18-MPGA-
646 0008).

647

648 References

- 649 Abril, G., Martinez, J. M., Artigas, L. F., Moreira-Turcq, P., Benedetti, M. F., Vidal, L., et al. (2014). Amazon River
650 carbon dioxide outgassing fuelled by wetlands. *Nature*, *505*(7483), 395–398.
651 <https://doi.org/10.1038/nature12797>
- 652 Alsdorf, D., Rodriguez, E., & Lettenmaier, D. P. (2007). Measuring surface water from space. *Reviews of*
653 *Geophysics*, *45*(2), 1–24. <https://doi.org/10.1029/2006RG000197>.1.INTRODUCTION
- 654 Alsdorf, D., Han, S. C., Bates, P., & Melack, J. (2010). Seasonal water storage on the Amazon floodplain measured
655 from satellites. *Remote Sensing of Environment*, *114*(11), 2448–2456.
656 <https://doi.org/10.1016/j.rse.2010.05.020>
- 657 Arcement Jr, G. J., & Schneider, V. R. (1989). Guide for Selecting Manning’s Roughness Coefficients for Natural
658 Channels and Flood Plains. *Technical Report, Geological Survey Water-Supply, United States Government*
659 *Printing Office, Washington, U.S.A*, 38. [https://doi.org/Report No. FHWA-TS-84-204](https://doi.org/Report%20No.%20FHWA-TS-84-204)
- 660 Armijos, E., Crave, A., Espinoza, J. C., Filizola, N., Espinoza-Villar, R., Ayes, I., et al. (2020). Rainfall control on
661 amazon sediment flux: Synthesis from 20 years of monitoring. *Environmental Research Communications*,
662 *2*(5). <https://doi.org/10.1088/2515-7620/ab9003>
- 663 Barbosa, C. C. F., Novo, E. M. L. de M., Melack, J. M., Freitas, R. M. de, & Pereira, W. (2006). A methodology for
664 analysis of volume and flooded area dynamics: Lago Grande de Curuai várzea as an example. *Revista*
665 *Brasileira de Cartografia*, *58*(3), 201–210.
- 666 Basso, L. S., Marani, L., Gatti, L. V., Miller, J. B., Gloor, M., Melack, J., et al. (2021). Amazon methane budget
667 derived from multi-year airborne observations highlights regional variations in emissions. *Communications*
668 *Earth & Environment*, *2*(1), 1–13. <https://doi.org/10.1038/s43247-021-00314-4>
- 669 Baugh, C. A., Bates, P. D., Schumann, G., & Trigg, M. A. (2013). SRTM vegetation removal and hydrodynamic
670 modeling accuracy. *Water Resources Research*, *49*(9), 5276–5289. <https://doi.org/10.1002/wrcr.20412>
- 671 Beighley, R. E., Eggert, K. G., Dunne, T., He, Y., Gummadi, V., & Verdin, K. L. (2009). Simulating hydrologic and
672 hydraulic processes throughout the Amazon River Basin. *Hydrological Processes*, *23*, 1221–1235.
673 <https://doi.org/10.1002/hyp>
- 674 Birkett, C. M., Mertes, L. A. K., Dunne, T., Costa, M. H., & Jasinski, M. J. (2002). Surface water dynamics in the
675 Amazon Basin: Application of satellite radar altimetry. *Journal of Geophysical Research D: Atmospheres*,

- 676 107(20). <https://doi.org/10.1029/2001JD000609>
- 677 Bonnet, M. P., Barroux, G., Martinez, J. M., Seyler, F., Moreira-Turcq, P., Cochonneau, G., et al. (2008). Floodplain
678 hydrology in an Amazon floodplain lake (Lago Grande de Curuaí). *Journal of Hydrology*, 349(1–2), 18–30.
679 <https://doi.org/10.1016/j.jhydrol.2007.10.055>
- 680 Bonnet, M. P., Pinel, S., Garnier, J., Bois, J., Resende Boaventura, G., Seyler, P., & Motta Marques, D. (2017).
681 Amazonian floodplain water balance based on modelling and analyses of hydrologic and electrical
682 conductivity data. *Hydrological Processes*, 31(9), 1702–1718. <https://doi.org/10.1002/hyp.11138>
- 683 Brunner, G. W. (2016). HEC-RAS river analysis system, User's Manual, Version 5.0. *US Army Corps of Engineers*
684 *Hydrologic Engineering Center, Davis CA*, (February), 960.
- 685 Callède, J., Cochonneau, G., Alves, F. V., Guyot, J.-L., Guimarães, V. S., & De Oliveira, E. (2010). The River
686 Amazon water contribution to the Atlantic Ocean. *Revue Des Sciences de l'eau*, 23(3), 247–273. Retrieved
687 from <https://www.erudit.org/en/journals/rseau/2010-v23-n3-rseau3946/044688ar/abstract/>
- 688 Cao, N., Lee, H., Jung, H. C., & Yu, H. (2018). Estimation of Water Level Changes of Large-Scale Amazon
689 Wetlands Using ALOS2 ScanSAR Differential Interferometry, 10(966). <https://doi.org/10.3390/rs10060966>
- 690 Chevuturi, A., Klingaman, N. P., Rudorff, C. M., Coelho, C. A. S., & Schöngart, J. (2022). Forecasting annual
691 maximum water level for the Negro River at Manaus. *Climate Resilience and Sustainability*, 1(1), 1–17.
692 <https://doi.org/10.1002/cli2.18>
- 693 Chow, V. Te. (1959). Open-channel hydraulics. *McGraw-Hill Book Company*, 728. [https://doi.org/ISBN 07-010776-](https://doi.org/ISBN 07-010776-9)
694 9
- 695 Coe, M. T., Costa, M. H., & Howard, E. A. (2008). Simulating the surface waters of the Amazon River basin:
696 Impacts of new river geomorphic and flow parameterizations. *Hydrological Processes*, 22(14), 2542–2553.
697 <https://doi.org/10.1002/hyp.6850>
- 698 Collischonn, W., Allasia, D., da Silva, B. C., & Tucci, C. E. M. (2007). The MGB-IPH model for large-scale
699 rainfall-runoff modelling. *Hydrological Sciences Journal*, 52(5), 878–895.
700 <https://doi.org/10.1623/hysj.52.5.878>
- 701 Correa, S. W., Paiva, R. C. D. de, Espinoza, J. C., & Collischonn, W. (2017). Multi-decadal Hydrological
702 Retrospective: Case study of Amazon floods and droughts. *Journal of Hydrology*, 549, 667–684.
703 <https://doi.org/10.1016/j.jhydrol.2017.04.019>
- 704 Dunne, T., Mertes, L. A. K., Meade, R. H., Richey, J. E., & Forsberg, B. R. (1998). Exchanges of sediment between
705 the flood plain and channel of the Amazon River in Brazil. *Geological Society of America Bulletin*,
706 110(December 1997), 450–467. [https://doi.org/10.1130/0016-7606\(1998\)110<0450](https://doi.org/10.1130/0016-7606(1998)110<0450)
- 707 Duponchelle, F., Isaac, V. J., Rodrigues Da Costa Doria, C., Van Damme, P. A., Herrera-R, G. A., Anderson, E. P.,
708 et al. (2021). Conservation of migratory fishes in the Amazon basin. *Aquatic Conservation: Marine and*
709 *Freshwater Ecosystems*, 31(5), 1087–1105. <https://doi.org/10.1002/aqc.3550>
- 710 Fassoni-Andrade, A. C., Paiva, R. C. D., Rudorff, C. M., Barbosa, C. C. F., & Novo, E. M. L. de M. (2020a). High-
711 resolution mapping of floodplain topography from space: A case study in the Amazon. *Remote Sensing of*
712 *Environment*, 251, 112065. <https://doi.org/10.1016/j.rse.2020.112065>
- 713 Fassoni-Andrade, A. C., Fleischmann, A. S., Paiva, R. C. D. (2020b). Lake topography and active storage from
714 satellite observations of flood frequency. *Water Resources Research*, 56(7). [https://doi.org/](https://doi.org/10.1029/2019wr026362)
715 10.1029/2019wr026362
- 716 Fassoni-Andrade, A. C., Fleischmann, A. S., Papa, F., Paiva, R. C. D. de, Wongchuig, S., Melack, J. M., et al.
717 (2021). Amazon Hydrology From Space: Scientific Advances and Future Challenges. *Reviews of Geophysics*,
718 59(4), 1–97. <https://doi.org/10.1029/2020RG000728>
- 719 Ferreira-Ferreira, J., Silva, T. S. F., Streher, A. S., Affonso, A. G., De Almeida Furtado, L. F., Forsberg, B. R., et al.
720 (2014). Combining ALOS/PALSAR derived vegetation structure and inundation patterns to characterize major
721 vegetation types in the Mamirauá Sustainable Development Reserve, Central Amazon floodplain, Brazil.
722 *Wetlands Ecology and Management*, 23(1), 41–59. <https://doi.org/10.1007/s11273-014-9359-1>
- 723 Filizola, N., Latrubesse, E. M., Fraizy, P., Souza, R., Guimarães, V., & Guyot, J. L. (2014). Was the 2009 flood the
724 most hazardous or the largest ever recorded in the Amazon? *Geomorphology*, 215, 99–105.
725 <https://doi.org/10.1016/j.geomorph.2013.05.028>
- 726 Fleischmann, A. S., Paiva, R. C. D., Collischonn, W., Sorribas, M. V., & Pontes, P. R. M. (2016). On river-
727 floodplain interaction and hydrograph skewness. *Water Resources Research*, 52(10), 7615–7630.
728 <https://doi.org/10.1002/2016WR019233>
- 729 Fleischmann, A. S., Paiva, R., & Collischonn, W. (2019). Can regional to continental river hydrodynamic models be
730 locally relevant? A cross-scale comparison. *Journal of Hydrology X*, 3, 100027.
731 <https://doi.org/10.1016/j.hydroa.2019.100027>

- 732 Fleischmann, A. S., Papa, F., Fassoni-Andrade, A., Melack, J. M., Wongchuig, S., Paiva, R. C. D. de, et al. (2022).
733 How much inundation occurs in the Amazon River basin? *Remote Sensing of Environment*, 278(June), 67.
734 <https://doi.org/10.1002/essoar.10508718.1>
- 735 Frappart, F., Papa, F., Güntner, A., Tomasella, J., Pfeffer, J., Ramillien, G., et al. (2019). The spatio-temporal
736 variability of groundwater storage in the Amazon River Basin. *Advances in Water Resources*, 124(October
737 2016), 41–52. <https://doi.org/10.1016/j.advwatres.2018.12.005>
- 738 Fricke, A. T., Nittrouer, C. A., Ogston, A. S., Nowacki, D. J., Asp, N. E., & Souza Filho, P. W. M. (2019).
739 Morphology and dynamics of the intertidal floodplain along the Amazon tidal river. *Earth Surface Processes
740 and Landforms*, 44(1), 204–218. <https://doi.org/10.1002/esp.4545>
- 741 Getirana, A. C. V., Boone, A., Yamazaki, D., Decharme, B., Papa, F., & Mognard, N. (2012). The Hydrological
742 Modeling and Analysis Platform (HyMAP): Evaluation in the Amazon Basin. *Journal of Hydrometeorology*,
743 13(6), 1641–1665. <https://doi.org/10.1175/JHM-D-12-021.1>
- 744 Hess, L. L., Melack, J. M., Novo, E. M. L. M. L. M., Barbosa, C. C. F. F., & Gastil, M. (2003). Dual-season
745 mapping of wetland inundation and vegetation for the central Amazon basin. *Remote Sensing of Environment*,
746 87(4), 404–428. <https://doi.org/10.1016/j.rse.2003.04.001>
- 747 Hess, L. L., Melack, J. M., Affonso, A. G., Barbosa, C., Gastil-Buhl, M., & Novo, E. M. L. M. (2015). Wetlands of
748 the Lowland Amazon Basin: Extent, Vegetative Cover, and Dual-season Inundated Area as Mapped with
749 JERS-1 Synthetic Aperture Radar. *Wetlands*, 35(4), 745–756. <https://doi.org/10.1007/s13157-015-0666-y>
- 750 Ji, X., Lesack, L. F. W., Melack, J. M., Wang, S., Riley, W. J., & Shen, C. (2019). Seasonal and inter-annual
751 patterns and controls of hydrological fluxes in an Amazon floodplain lake with a surface-subsurface processes
752 model. *Water Resources Research*, 55(4), 3056–3075. <https://doi.org/10.1029/2018WR023897>
- 753 Latrubesse, E. M., & Franzinelli, E. (2002). The Holocene alluvial plain of the middle Amazon River, Brazil.
754 *Geomorphology*, 44(3–4), 241–257. [https://doi.org/10.1016/S0169-555X\(01\)00177-5](https://doi.org/10.1016/S0169-555X(01)00177-5)
- 755 LeFavour, G., & Alsdorf, D. (2005). Water slope and discharge in the Amazon River estimated using the shuttle
756 radar topography mission digital elevation model. *Geophysical Research Letters*, 32(17), 1–5.
757 <https://doi.org/10.1029/2005GL023836>
- 758 Lesack, F. W., & Melack, J. M. (1995). Flooding hydrology and mixture dynamics of lakewater derived from
759 multiple sources in an Amazon floodplain lake. *Water Resources Research*, 31(2), 329–345.
- 760 Luo, X., Li, H. Y., Ruby Leung, L., Tesfa, T. K., Getirana, A., Papa, F., & Hess, L. L. (2017). Modeling surface
761 water dynamics in the Amazon Basin using MOSART-Inundation v1.0: Impacts of geomorphological
762 parameters and river flow representation. *Geoscientific Model Development*, 10(3), 1233–1259.
763 <https://doi.org/10.5194/gmd-10-1233-2017>
- 764 Melack, J. M., Novo, E. M. L. M., Forsberg, B. R., Piedade, M. T. F. F., & Maurice, L. (2009). Floodplain
765 Ecosystem Processes. *Amazonia and Global Change*, (2003), 525–541.
766 <https://doi.org/10.1029/2008GM000727>
- 767 Paiva, R. C. D. de, Buarque, D. C., Collischonn, W., Bonnet, M. P., Frappart, F., Calmant, S., & Bulhões Mendes,
768 C. A. (2013). Large-scale hydrologic and hydrodynamic modeling of the Amazon River basin. *Water
769 Resources Research*, 49(3), 1226–1243. <https://doi.org/10.1002/wrcr.20067>
- 770 Papa, F., Frappart, F., Güntner, A., Prigent, C., Aires, F., Getirana, A. C. V., & Maurer, R. (2013). Surface
771 freshwater storage and variability in the Amazon basin from multi-satellite observations, 1993–2007. *Journal
772 of Geophysical Research Atmospheres*, 118(21), 11951–11965. <https://doi.org/10.1002/2013JD020500>
- 773 Pinel, S., Bonnet, M.-P., Santos Da Silva, J., Moreira, D., Calmant, S., Satgé, F., & Seyler, F. (2015). Correction of
774 Interferometric and Vegetation Biases in the SRTMGL1 Spaceborne DEM with Hydrological Conditioning
775 towards Improved Hydrodynamics Modeling in the Amazon Basin. *Remote Sensing*, 7(12), 16108–16130.
776 <https://doi.org/10.3390/rs71215822>
- 777 Pinel, S., Bonnet, M., Silva, J. S. Da, Sampaio, T. C., Garnier, J., Catry, T., et al. (2019). Flooding dynamics within
778 a Amazonian floodplain : Water circulation patterns and inundation duration. *Water Resources Research*,
779 56(1). <https://doi.org/10.1029/2019WR026081>
- 780 Richey, J. E., Mertes, L. K., Dunne, T., Victoria, R. L., Forsberg, B. R., Tancredi, A. C. N. S., & Oliveira, E. de.
781 (1989). Sources and routing of the Amazon River flood wave, 3(3), 191–204.
- 782 Rosenqvist, J., Rosenqvist, A., Jensen, K., & McDonald, K. (2020). Mapping of maximum and minimum inundation
783 extents in the amazon basin 2014–2017 with ALOS-2 PALSAR-2 scan SAR time-series data. *Remote Sensing*,
784 12(8). <https://doi.org/10.3390/RS12081326>
- 785 Rudorff, C. M., Melack, J. M., & Bates, P. D. (2014a). Flooding dynamics on the lower Amazon floodplain: 1.
786 Hydraulic controls on water elevation, inundation extent, and river-floodplain discharge. *Water Resources
787 Research*, 50(1), 619–634. <https://doi.org/10.1002/2013WR014091>

- 788 Rudorff, C. M., Melack, J. M., & Bates, P. D. (2014b). Flooding dynamics on the lower Amazon floodplain: 2.
789 Seasonal and interannual hydrological variability. *Water Resources Research*, 50(1), 635–649.
790 <https://doi.org/10.1002/2013WR014714>
- 791 Schumann, G., Bates, P. D., Horritt, M. S., Matgen, P., & Pappenberger, F. (2009). Progress in Integration of
792 Remote Sensing-Derived Flood Extent and Stage Data and Hydraulic Models. *Reviews of Geophysics*,
793 47(2008), 1–20. <https://doi.org/10.1029/2008rg000274>
- 794 Silva, J. S. Da, Calmant, S., Seyler, F., Rotunno Filho, O. C., Cochonneau, G., & Mansur, W. J. (2010). Water levels
795 in the Amazon basin derived from the ERS 2 and ENVISAT radar altimetry missions. *Remote Sensing of*
796 *Environment*, 114(10), 2160–2181. <https://doi.org/10.1016/j.rse.2010.04.020>
- 797 Siqueira, V. A., Paiva, R. C. D., Fleischmann, A. S., Fan, F. M., Ruhoff, A. L., Pontes, P. R. M., et al. (2018).
798 Toward continental hydrologic-hydrodynamic modeling in South America. *Hydrology and Earth System*
799 *Sciences*, 22(9), 4815–4842. <https://doi.org/10.5194/hess-22-4815-2018>
- 800 Sorribas, M. V., de Paiva, R. C. D., Fleischmann, A. S., & Collischonn, W. (2020). Hydrological Tracking Model
801 for Amazon Surface Waters. *Water Resources Research*, 56(9), 1–19. <https://doi.org/10.1029/2019WR024721>
- 802 Trigg, M. A., Wilson, M. D., Bates, P. D., Horritt, M. S., Alsdorf, D. E., Forsberg, B. R., & Vega, M. C. (2009).
803 Amazon flood wave hydraulics. *Journal of Hydrology*, 374(1–2), 92–105.
804 <https://doi.org/10.1016/j.jhydrol.2009.06.004>
- 805 Trigg, M. A., Bates, P. D., Wilson, M. D., Schumann, G., & Baugh, C. (2012). Floodplain channel morphology and
806 networks of the middle Amazon River. *Water Resources Research*, 48(10), 1–17.
807 <https://doi.org/10.1029/2012WR011888>
- 808 Tull, N., Passalacqua, P., Hassenruck-Gudipati, H. J., Rahman, S., Wright, K., Hariharan, J., & Mohrig, D. (2022).
809 Floodplain Connectivity During Combined Pluvial-Fluvial Events. *Water Resources Research*, 58(3), 1–24.
810 <https://doi.org/10.1029/2021WR030492>
- 811 Wilson, M. D., Bates, P., Alsdorf, D., Forsberg, B., Horritt, M., Melack, J., et al. (2007). Modeling large-scale
812 inundation of Amazonian seasonally flooded wetlands. *Geophysical Research Letters*, 34(15), 4–9.
813 <https://doi.org/10.1029/2007GL030156>
- 814 Wohl, E. (2021). An Integrative Conceptualization of Floodplain Storage. *Reviews of Geophysics*, 59(2), 1–63.
815 <https://doi.org/10.1029/2020RG000724>
- 816 Yamazaki, D., Kanae, S., Kim, H., & Oki, T. (2011). A physically based description of floodplain inundation
817 dynamics in a global river routing model. *Water Resources Research*, 47(4).
818 <https://doi.org/10.1029/2010WR009726>
- 819 Yamazaki, D., Baugh, C. A., Bates, P. D., Kanae, S., Alsdorf, D. E., & Oki, T. (2012). Adjustment of a spaceborne
820 DEM for use in floodplain hydrodynamic modeling. *Journal of Hydrology*, 436–437, 81–91.
821 <https://doi.org/10.1016/j.jhydrol.2012.02.045>
- 822 Yamazaki, D., Lee, H., Alsdorf, D. E., Dutra, E., Kim, H., Kanae, S., & Oki, T. (2012). Analysis of the water level
823 dynamics simulated by a global river model: A case study in the Amazon River. *Water Resources Research*,
824 48(9), 1–15. <https://doi.org/10.1029/2012WR011869>
- 825 Yamazaki, D., Ikeshima, D., Tawatari, R., Yamaguchi, T., O’Loughlin, F., Neal, J. C., et al. (2017). A high-
826 accuracy map of global terrain elevations. *Geophysical Research Letters*, 44(11), 5844–5853.
827 <https://doi.org/10.1002/2017GL072874>
- 828 Zhang, Q., & Werner, A. D. (2015). Hysteretic relationships in inundation dynamics for a large lake-floodplain
829 system. *Journal of Hydrology*, 527, 160–171. <https://doi.org/10.1016/j.jhydrol.2015.04.068>
- 830

Water Resources Research

Supporting Information for

Expressive riverine fluxes over Amazon floodplain units revealed by high resolution 2D modelling

Alice César Fassoni-Andrade^{1,2*}, Rodrigo Cauduro Dias de Paiva¹, Sly Wongchuig³, Claudio Barbosa⁴, Fabien Durand^{2,5}

¹ Institute of Hydraulic Research, Federal University of Rio Grande do Sul (UFRGS), Porto Alegre, Brazil.

² Institute of Geosciences, University of Brasília (UnB), Campus Universitário Darcy Ribeiro, Brasília, Brazil.

³ Univ. Grenoble Alpes, IRD, CNRS, Grenoble INP, Institut des Géosciences de l'Environnement (IGE, UMR 5001), 38000, Grenoble, France.

⁴ Instrumentation Lab for Aquatic Systems (LabISA), Earth Observation Coordination of National Institute for Space Research (INPE), São José dos Campos, SP, Brazil.

⁵ Laboratoire d'Etudes en Géophysique et Océanographie Spatiales (LEGOS), Université Toulouse, IRD, CNRS, CNES, UPS, Toulouse, France.

Contents of this file

Table S1

Table S2

Table S3

Introduction

In this supporting information, we provide detailed information on in situ and virtual stations used in the modeling (Table S1), area proportion of Manning's roughness coefficients class to the computational domain (Table S2), and water surface elevation metrics evaluated at Amazon River stations (Table S3).

Table S1 Name, code, and location of in situ stations operated by Agência Nacional de Águas e Saneamento Básico (ANA) and virtual stations available in Hydroweb

Name	Code	Source	Latitude	Longitude
Manacapuru	14100000	ANA	-3.308	-60.609
Porto de Moz	18950003	ANA	-1.753	-52.241
Moura	14840000	ANA	-1.456	-61.634
Jatuarana	15030000	ANA	-3.052	-59.678
Parintins	16350002	ANA	-2.630	-56.752
Santarém	17900000	ANA	-2.416	-54.716
Curuai	17060000	ANA	-2.268	-55.481
Óbidos	17050001	ANA	-1.947	-55.511
amz_amz_env_	0020_01	Hydroweb	-3.161	-59.465
amz_amz_env_	0063_01	Hydroweb	-3.338	-58.774
amz_amz_env_	0220_01	Hydroweb	-2.391	-54.266
amz_amz_env_	0263_01	Hydroweb	-2.083	-54.020
amz_amz_env_	0306_01	Hydroweb	-1.907	-55.596
amz_amz_env_	0349_01	Hydroweb	-1.946	-55.487
amz_amz_env_	0392_01	Hydroweb	-2.533	-57.171
amz_amz_env_	0435_01	Hydroweb	-2.611	-56.778
amz_amz_env_	0478_02	Hydroweb	-3.331	-58.784
amz_amz_env_	0521_01	Hydroweb	-2.953	-58.14
amz_amz_env_	0607_01	Hydroweb	-3.125	-59.539
amz_amz_env_	0764_01	Hydroweb	-2.146	-54.930
amz_amz_env_	0807_01	Hydroweb	-2.405	-54.668
amz_amz_env_	0850_01	Hydroweb	-2.368	-56.416
amz_amz_env_	0893_01	Hydroweb	-2.123	-56.167
amz_amz_env_	0936_01	Hydroweb	-2.798	-57.948
amz_amz_env_	0979_01	Hydroweb	-2.407	-57.542
R_amz_amz_jas_	0139_01	Hydroweb	-2.571	-56.897
R_amz_amz_jas_	0152_01	Hydroweb	-3.254	-59.068
R_amz_amz_jas_	0228_01	Hydroweb	-2.488	-56.508
R_amz_amz_jas_	0063_01	Hydroweb	-3.281	-59.985

Table S2 Manning's roughness coefficients adopted in each class of the mapping of Hess et al. (2015) and proportion of the area occupied in the computational domain

Class	Description (Hess et al., 2003)	Mapping code (Hess et al., 2015)	Manning's roughness coefficients	Spatial proportion in the domain*
Open water	Lago, paran, igarap, furo	11 13	0.022 (Same as the river)	17%
Bare soil or herbaceous	Terreno aberto, campo, macrfitas aquticas	21 23 33	0.03	18%
Shrub	Vegetao arbustiva, campina	41 44 45 51 55	0.04	11%
Woodland	Chavascal, pntano, savanas inundadas	66 67 77	0.14	27.3%
Forest	Floresta, mata	88 89 99	0.14	4.4%
Terra firme	Fora da plancie de inundao	-	0.18	9.1%

*13.2% of the area represents the Amazon River.

Other studies have based on Hess' mapping assigning similar Manning's coefficient values. Rudorff et al. (2014a) used 0.14 and 0.10 for the forest and shrub vegetation classes. Pinel et al. (2019) assigned 0.032 for permanent water, 0.042 for shrub vegetation, 0.14 for flooded forest, and 0.18 for forested areas.

References:

- Hess, L.L., Melack, J.M., Affonso, A.G., Barbosa, C., Gastil-Buhl, M., Novo, E.M.L.M., 2015. Wetlands of the Lowland Amazon Basin: Extent, Vegetative Cover, and Dual-season Inundated Area as Mapped with JERS-1 Synthetic Aperture Radar. *Wetlands* 35, 745–756. <https://doi.org/10.1007/s13157-015-0666-y>
- Hess, L.L., Melack, J.M., Novo, E.M.L.M.L.M., Barbosa, C.C.F.F., Gastil, M., 2003. Dual-season mapping of wetland inundation and vegetation for the central Amazon basin. *Remote Sens. Environ.* 87, 404–428. <https://doi.org/10.1016/j.rse.2003.04.001>
- Pinel, S., Bonnet, M., Silva, J.S. Da, Sampaio, T.C., Garnier, J., Catry, T., Calmant, S., Jr, C.R.F., Moreira, D., Marques, D.M., Seyler, F., 2019. Flooding dynamics within a Amazonian floodplain : Water circulation patterns and inundation duration. *Water Resour. Res.* 56. <https://doi.org/10.1029/2019WR026081>
- Rudorff, C.M., Melack, J.M., Bates, P.D., 2014. Flooding dynamics on the lower Amazon floodplain: 1. Hydraulic controls on water elevation, inundation extent, and river-floodplain discharge. *Water Resour. Res.* 50, 619–634. <https://doi.org/10.1002/2013WR014091>

Table S3 Water surface elevation metrics evaluated at Amazon River stations

Station	Number of data	Bias	RMSE	NSE	<i>r</i>
0020_01	28	-0.86	1.38	0.82	0.94
0063_01	29	-0.43	0.58	0.97	1.00
0220_01	29	-0.42	0.48	0.93	0.99
0263_01	30	-0.40	0.48	0.92	0.99
0306_01	31	-0.60	1.01	0.83	0.95
0349_01	29	-0.47	0.62	0.93	0.99
0392_01	31	-1.28	1.54	0.61	0.95
0435_01	30	-0.47	0.62	0.95	0.99
0478_02	31	-0.36	0.51	0.98	1.00
0521_01	30	-0.48	0.61	0.96	0.99
0607_01	29	-0.13	0.45	0.99	0.99
0764_01	29	-0.59	0.70	0.85	0.98
0807_01	29	-0.82	1.02	0.64	0.96
0850_01	31	-0.59	0.67	0.94	1.00
0893_01	31	-0.83	0.99	0.84	0.98
0936_01	29	-0.75	0.80	0.93	1.00
0979_01	31	-0.47	0.68	0.95	0.99
0139_01	81	-0.68	1.38	0.45	0.95
0152_01	75	0.00	0.61	0.96	0.98
0228_01	82	-0.50	0.94	0.81	0.97
0063_01	74	-0.15	0.64	0.98	0.99
Curuai	1005	0.65	0.67	0.92	1.00
Óbidos	1066	0.30	0.37	0.98	1.00